ACTINIDE RESEARCH QUARTERLY
Los Alamos National Laboratory
Issue 3 • December 2013

89 Ac | 90 Th | 91 Pa | 92 U | 93 Np | 94 Pu | 95 Am | 96 Cm | 97 Bk | 98 Cf | 99 Es | 100 Fm | 101 Md | 102 No | 103 Lr

2013 GLENN T. SEABORG INSTITUTE POSTDOCS

> ***Postdocs are the technical vitality*** *of the research at LANL*

LA-UR-13-29395

Fostering Excellence and External Visibility in Actinide Science

The primary mission of the Los Alamos National Laboratory is national security. While this mission has remained constant throughout the Laboratory's 70-year history, the challenges to national security have changed and our technical work has evolved to meet these challenges. The Laboratory's mission space has been broadly categorized into nuclear deterrence, energy security, and global threat reduction. The science and technology of the actinide elements support all these mission areas. The importance and challenges of actinide science are well described in the *Integrated Plutonium Science and Research Strategy* (LAUR-13-24336) recently issued jointly by the Los Alamos and the Lawrence Livermore national laboratories.

The Glenn T. Seaborg Institute branches at Los Alamos, Livermore, and Lawrence Berkeley-University of California, Berkeley, were chartered by the University of California and established by the individual Laboratory Directors to promote excellence in actinide science and to attract a future generation of actinide scientists and engineers. Here at Los Alamos, the Seaborg Institute has developed a Postdoctoral Fellows program as an important component of mission. With funding from the Laboratory Directed Research and Development (LDRD) Program and the Strategic Outcomes Office of the Global Security Directorate, 12–16 postdoctoral researchers are supported at half-time. The Seaborg Fellows must be approved as Los Alamos postdocs and are selected in a competitive review of their proposed work and its relevance to Los Alamos actinide science and their research and academic record. The research of the Fellows fosters sustained excellence and external visibility in actinide science at Los Alamos. The Seaborg Fellows have been members of many divisions, including Materials Science and Technology, Chemistry, Theoretical, Nuclear Engineering and Nonproliferation, and Materials Physics and Applications. About 25% of the Fellows have become permanent technical staff at the Laboratory. We highlight some of their research in this issue of the ARQ.

Albert Migliori, *Director*
Gordon Jarvinen, *Deputy Director*
Glenn T. Seaborg Institute

Table of Contents

About the cover:
This issue of ARQ presents research of seven current, or recent, Los Alamos National Laboratory Glenn T. Seaborg Institute postdocs. Since the founding of the Seaborg Institute at Los Alamos in 1997, more than 70 promising PhDs have been awarded Seaborg Institute fellowships. LANL Seaborg postdocs have gone on to research and teaching positions here at LANL, in the US, and internationally. The cover quote is from Mary Anne With, Office Leader, LANL Postdoc Program.

David Anderssen

David Anderssen was a LANL Seaborg postdoc from February 2008–October 2009, now working in Materials Science and Technology (MST-8). His field of study is theoretical modeling of nanoscale heterogeneity in Pu/U alloys and oxides. His mentor was Steve Conradson of MST-8.

Modeling Oxidation of Actinide Dioxides by Density Functional Theory Calculations

We have investigated oxidation of actinide dioxides such as UO_2, NpO_2, and PuO_2 using density functional theory (DFT) calculations. DFT calculations derive the forces between atoms that govern their internal arrangement and motion from the density distribution of electrons as determined by the laws of quantum mechanics. This methodology is a powerful tool for studying materials and how they are influenced by changes in chemistry that may occur due to exposure to, for example, oxygen-rich atmospheres or water. It applies to discovering structural (the configuration of atoms), thermodynamic (the stability of these configurations), or kinetic (diffusion of atoms) properties.

UO_2 is probably the most important compound among the actinide dioxides due to its application as nuclear reactor fuel in light water reactors. Other actinides exist in fuels as fission products, and some reactors use reprocessed mixed oxide (MOX) fuels with significant concentrations of PuO_2.

Oxidation of actinide dioxides emerges as a central theme in fuel fabrication, reactor operation, long-term storage forms for both spent fuels and surplus weapons materials, and environmental actinide migration. One of the most critical properties for the performance of nuclear fuels is the release of fission gases, especially the noble gases xenon (Xe) and krypton (Kr).

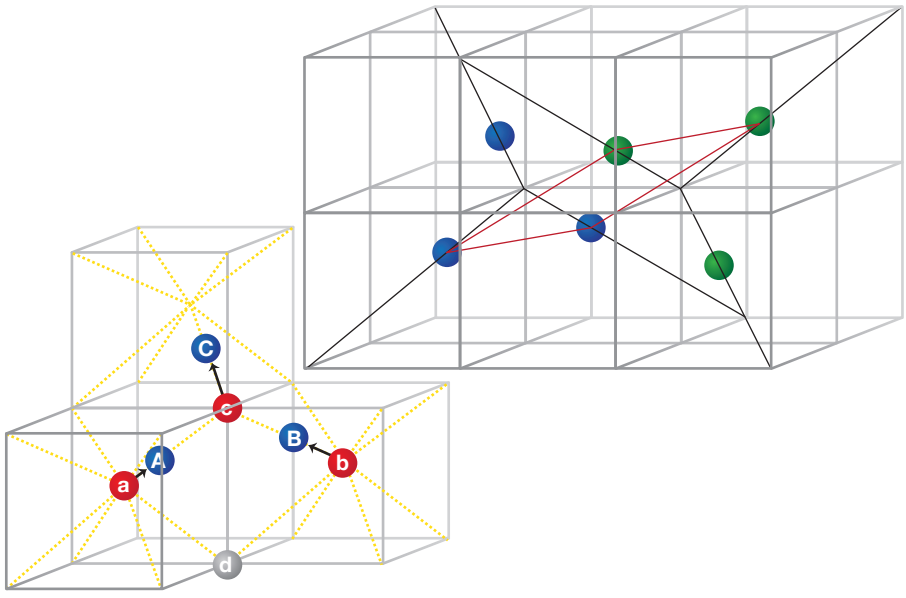

Figure 1: Idealized schematic of the di-interstitial cluster (red) and split di-interstitial cluster (blue). The arrows indicate how the oxygen ions relax to form the more stable split di-interstitial cluster. (Right) Idealized schematic of the split quadinterstitial oxygen cluster. The two split di-interstitials that make up the quadinterstitial are highlighted in blue and green, respectively. In both figures the cubes represent the simple-cubic oxygen sublattice; for clarity, U ions are not shown.

Transport of these gases within the fuel is usually the rate-limiting step and it occurs by migration assisted by uranium vacancies. The concentration of uranium vacancies is directly controlled by the oxygen content of the fuel and, consequently, understanding oxidation of UO_2 is a prerequisite for being able to predict the release rate of fission gases. The oxidation of actinide dioxides is also of fundamental interest in actinide science, since it is closely coupled to the properties of the 5*f* electrons that are the source of the complexities of actinide materials.

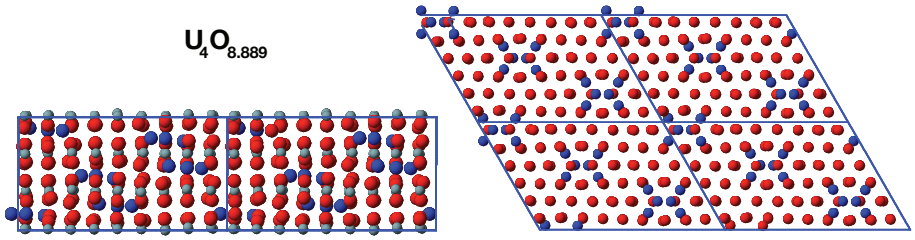

Figure 2: Two different views of the lowest energy structure of U_4O_{9-y} ($U_4O_{8.889}$) obtained from DFT. Red spheres represent regular oxygen ions; gray spheres represent uranium ions. The cluster ions are highlighted in blue.

The oxidation properties of actinide dioxides demonstrate significant variability within the actinide series of compounds, e.g., while UO_2 easily reacts with oxygen, the transuranic oxides such as PuO_2 are less prone to oxidation. PuO_2 seems to require special conditions in order to accommodate excess oxygen. These properties are all related to the unique behavior of the actinide 5*f* electrons and the unusually high degree of covalent mixing or hybridization in chemical bonds between oxygen and actinides. Upon oxidation, UO_{2+x} retains the parent fluorite crystal structure up to the U_4O_9 compound and, under some conditions, all the way to U_3O_7. Both of these compounds exhibit an ordered arrangement of interstitial-like oxygen ions within the parent fluorite lattice. However, the structures are very complicated large unit cells containing several hundred atoms. The ability of the fluorite lattice in UO_2 to accommodate excess oxygen ions is rather fascinating. The crystal lattice constant only changes from 5.47 Å to 5.45 Å between UO_2 and U_4O_9, and small distortions of the cubic crystal first emerge in U_3O_7. PuO_2 was long thought to be the highest stable oxide of plutonium, however, Haschke and collaborators reported in Science that PuO_2 reacts with moist air to form PuO_{2+x}.[1] Subsequent EXAFS (extended X-ray absorption fine structure) studies by Conradson and collaborators demonstrated that PuO_{2+x} is more accurately represented as a compound containing OH^- and H_2O species.[2] NpO_{2+x} compounds that are derived from the NpO_2 fluorite lattice have not been reported in the literature, and the experimental phase diagram points to a two-phase field that involves NpO_2 and Np_2O_5 below 700 K. We would like to better understand the complex behavior of UO_2 oxidation, in particular the ability to accommodate high concentrations of oxygen ions and their preferred binding geometry, as well as why NpO_2 and PuO_2 differ from the uranium-oxygen system. We approached this problem by performing computer simulations of the UO_2, NpO_2, and PuO_2 oxidation process. DFT calculations were used to study the structure, thermodynamic stability, and electronic characteristics of interstitial oxygen clusters in these compounds and how these clusters may order at the A_4O_9 (A denotes U, Np, or Pu) composition. For UO_{2+x} oxidation was simulated up to U_3O_8,

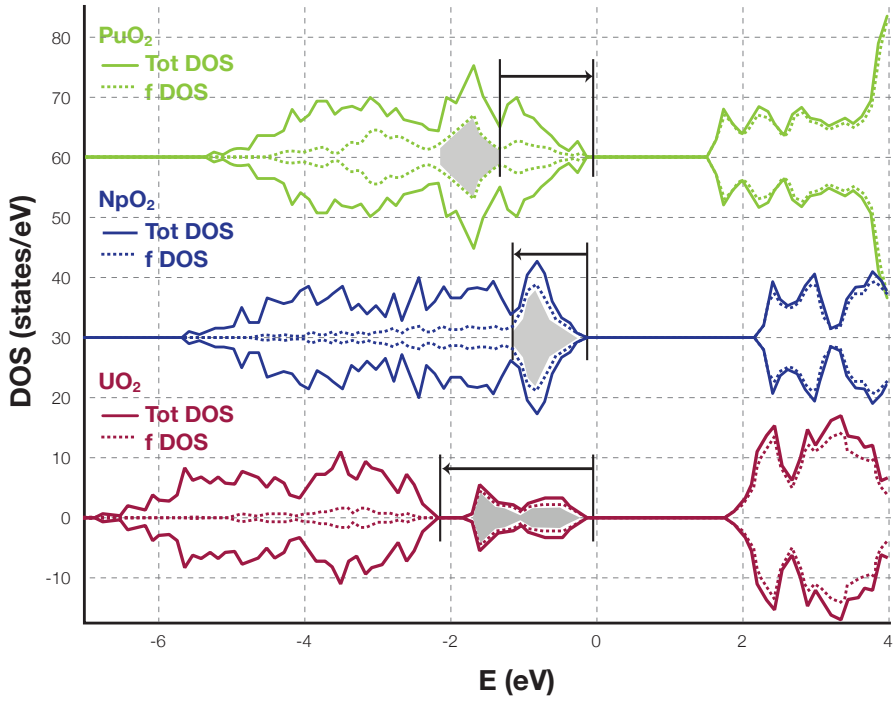

Figure 3: The density of states of UO_2, NpO_2, and PuO_2. The position of the actinide 5f bands is shown in dashed lines, including both localized states (shaded in gray) and states hybridized with the O 2p band. The arrows indicate the separation of the localized A 5f states and the O 2p bands, which drives the oxidation thermodynamics.

which is the first compound deviating significantly from the fluorite structure upon oxidation. The role of H_2O and OH^- in the oxidation process was also addressed.

Theoretical studies of actinide dioxides are complicated by the strongly correlated nature of actinide 5*f* electrons, which cause conventional exchange-correlation functionals (used to capture the electron-electron interactions in DFT calculations) to describe actinide dioxides as ferromagnetic metals instead of the antiferromagnetic Mott insulators that are found in experiments. However, there are several approaches to address this issue, such as the DFT+U method and hybrid density functionals. We have applied the DFT+U methodology in our studies due to its higher computational efficiency compared with the alternatives. This is required for describing the large clusters of oxygen ions in AO_{2+x} and, for example, the large unit cells of the ordered U_4O_9 and U_3O_7 compounds.

Oxidation means that oxygen atoms are inserted into the empty holes of the fluorite AO_2 lattice. One of the intriguing characteristics of hyperstoichiometric actinide dioxides (AO_{2+x}) is that the oxygen ions interact very strongly with each other and form clusters of interstitial oxygen ions. Over the years, different models (for example, the Willis cluster, the cuboctahedral cluster, and the short oxo-bonds found in molecular uranium-oxygen complexes) have been proposed for the geometry of these clusters based on neutron diffraction and X-ray spectroscopy measurements. The nature of the bonds between the excess oxygen ions and the AO_2 lattice is still not firmly established. Using DFT calculations to address this problem, we found the so-called split di-interstitial, illustrated in Fig. 1, to be the fundamental building block of the defect clusters. The most stable configuration constitutes two split di-interstitials that are rotated 180° with

respect to each other (see Fig. 1). Our calculations demonstrate that the stability of these clusters is a consequence of the increased bonding between the actinide ions and the excess oxygen ions. We have also predicted a new ground-state structure for U_4O_9 (see Fig. 2) that is based on a superstructure or ordered pattern of split quad-interstitials. The exact composition of this compound is slightly substoichiometric (U_4O_{9-y}), which agrees with experiments. The structure is controlled by ordering of the very stable quad-interstitial clusters to create as much separation as possible between the individual clusters. The same rule applies to the most stable structure of U_3O_7.

The structural insights acquired from these DFT calculations allow us to assess the oxidation thermodynamics of UO_2, NpO_2, and PuO_2. UO_2 exhibits strongly negative oxidation energy and reacts readily with oxygen, while NpO_2 is significantly harder to oxidize, and PuO_2 is predicted to have positive, or just slightly negative, oxidation energy. The degree of AO_2 oxidation is a function of the position of the actinide 5*f* electrons relative to the O 2p band. If these states are situated above the O 2p band, oxidation easily occurs (UO_2), while the overlap of actinide 5*f* and O 2p states in PuO_2 suppresses oxidation (see Fig. 3). The presence of H_2O is able to offset this effect and turn oxidation of PuO_2 into an exothermic process, which agrees with the experimental picture. We have seen that oxidation of UO_2 leads to formation of the ordered U_4O_9 and U_3O_7 compounds. Above a U:O ratio of 3:7 the fluorite structure is not able to incorporate more oxygen ions and instead transforms to U_3O_8. Although the transition from fluorite to the layered U_3O_8 structure occurs at U_3O_7 or $U_3O_{7.333}$, our calculations indicate that the fluorite-derived compounds are favored up to $UO_{2.5}$; that is, as long as the charge-compensation for adding oxygen atoms occurs via formation of U^{5+} ions;. as soon as U^{6+} ions are created, the U_3O_{8-y} phase becomes more stable.

In summary, we applied DFT calculations to study oxidation of actinide dioxides; the reactivity was shown to be controlled by the properties of their f electrons. Similar techniques were used to identify new structure models for UO_{2+x} and the ordered U_4O_9 and U_3O_7 compounds.

Acknowledgement

This work was funded by the Glenn T. Seaborg Institute and the Laboratory-directed Research and Development (LDRD) program at Los Alamos National Laboratory.

References:

[1]J.M. Haschke, T.H. Allen, L.A. Morales, "Reaction of Plutonium Dioxide with Water: Formation and Properties of PuO_{2+x}", Science 287(5451) (2000).

[2]S.D. Conradson, B.D. Begg, D.L. Clark, C.D. Auwer, F.J. Espinosa-Faller, P.L. Gordon, N J. Hess, R. Hess, D.W. Keogh, L.A. Morales, M.P. Neu, W.Runde, C.D. Tait, D.K. Veirs, P.M. Villella, "Speciation and Unusual Reactivity in PuO_{2+x}", Inorg. Chem. 42, 3715 (2003).

Further reading:

D.A. Andersson, J. Lezama, B.P. Uberuaga and S.D. Conradson, "Cooperativity among defect sites in AO_{2+x} and A_4O_9 (A=U,Np,Pu): Density functional calculations", Phys. Rev. B 79, 024110 (2009).

D.A. Andersson, T. Watanabe, C. Deo, and B.P. Uberuaga, "Role of di-interstitial clusters in oxygen transport in UO_{2+x} from first principles", Phys. Rev. B 80, 060101(R) (2009).

D.A. Andersson, F.J. Espinosa-Faller, B.P. Uberuaga and S.D. Conradson, "Stability and migration of large oxygen clusters in UO_{2+x}: Density functional theory calculations", J. Chem. Phys. 136, 234702 (2012).

D.A. Andersson, G. Baldinozzi, L. Desgranges, D.R. Conradson and S.D. Conradson, "Density Functional Theory Calculations of UO_2 Oxidation: Evolution of UO_{2+x}, U_4O_{9-y}, U_3O_7, and U_3O_8", Inorg. Chem. 52, 2769 (2013).

Xiao-Yan Chen

This paper was contributed by Xiao-Yan Chen, George S. Goff, Brian L. Scott, and Wolfgang Runde. Runde and Goff of C-IIAC, are her mentors. Her area of interest is actinide chemistry in functionalized ionic liquids. Xiao-Yan was a Seaborg postdoc from Aril 2012--October 2013 and has accepted a position outside the Laboratory.

Coordination Chemistry of Alpha-Hydroxyisobutyric Acid with *4f* Elements

Alpha-hydroxyisobutyric acid (HIBA, $C_4H_8O_3$, CAS# 565-70-8) is an important chemical with a wide range of applications including biodegradable plastics, cleaning agents, food additives, and pharmaceutical formulations. HIBA was first used in 1956 as a superior reagent to separate individual members of the lanthanide series (Ref. 1) from a complex mixture using a Dowex™ 50 cation-exchange resin and soon after was identified as an efficient separation reagent for the discovery of the transplutonium elements (Ref. 2). Although many chelating agents have been tested and used for lanthanide chromatographic separations, HIBA remains the premier separating reagent. The hydroxyl and carboxyl functionality enables various coordination modes for HIBA, in which the hydroxyl group can be either protonated or deprotonated. Despite that HIBA has been used as an eluent to separate lanthanides and actinides for many years, the eluted products in solution were generally not structurally characterized, and information on the coordination of lanthanides with HIBA remains rare. The dual hydroxyl and carboxyl functionality enables various coordination modes for HIBA (Scheme 1). Several researchers have reported that HIBA most likely forms negatively charged solution complexes with the lanthanides of the general formula $Ln(HIBA)_4^-$ (Ref. 3-5), There is only one reported crystal structure of a lanthanide with HIBA: $La(HIBA)_2 \cdot Cl \cdot 2H_2O$. The authors described this as a one-dimensional polymeric chain in which eight-coordinate La(III) atoms are connected via bridging carboxyl groups. Based on powder X-ray diffraction data, the authors hypothesize the existence of two different structure types across the lanthanide series with the structural break at Pr(III). Unfortunately, the authors did not provide any details of the powder X-ray diffraction analysis and failed to elaborate on the nature of the proposed second lanthanide-HIBA complex (Ref. 6).

Over the last few years our research group has focused on developing a fundamental understanding of lanthanide and actinide solubility and speciation in nonconventional environments to exploit their differences for actinide and lanthanide separations. Since HIBA can form complexes with both lanthanides and actinides, it is critical to understand the coordination chemistry of HIBA with the f-elements. In order to fill this knowledge gap, we studied the solution-state and solid-state coordination chemistry of HIBA across the lanthanide series. The reaction of lanthanides with HIBA at

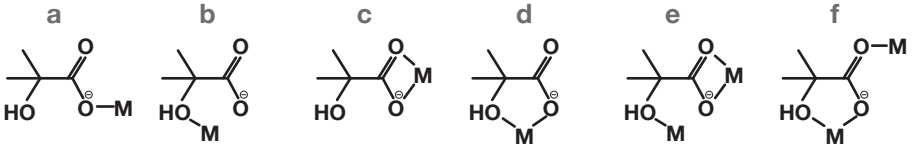

Scheme 1: Some of the possible coordination modes of HIBA ligand.

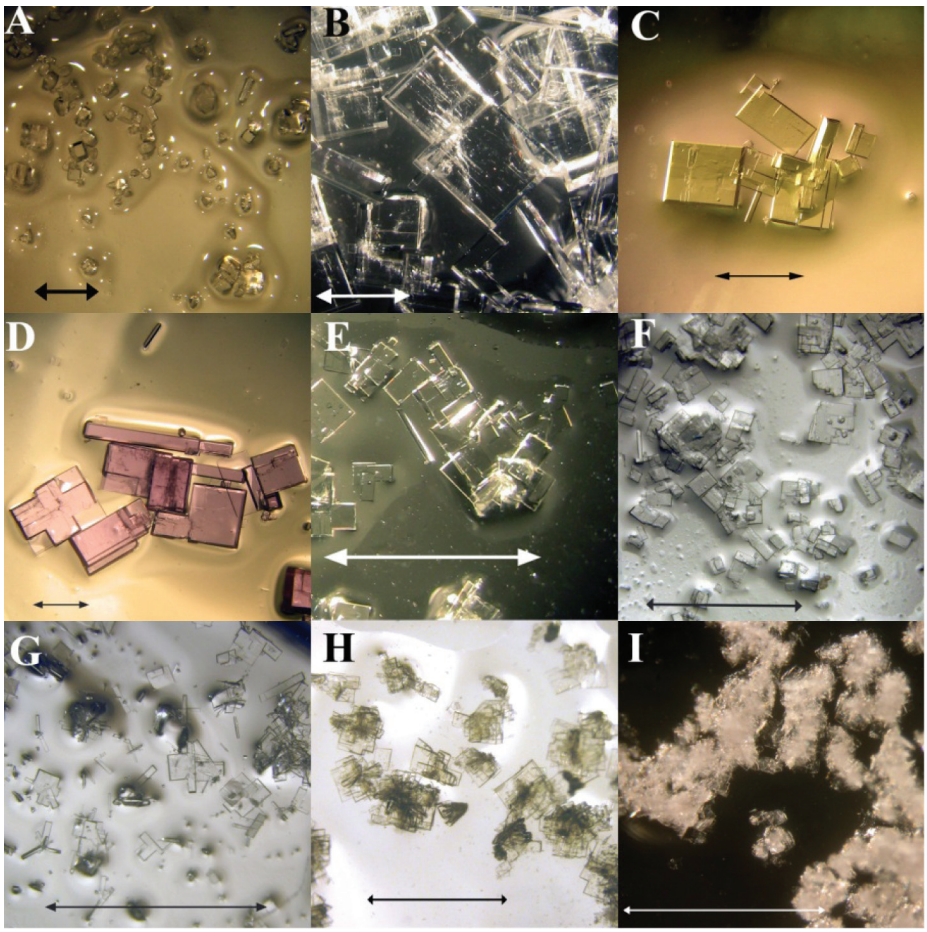

Figure 1: Photographs of single crystals $[Ln(HIBA)_2(H_2O)_2](NO_3)\cdot H_2O$, Ln = La (A), Ce (B), Pr (C), Nd (D), Sm (E), Eu (F), Gd (G), Ho (H), and Er (I). The scale shows a 1-mm arrow for A-G and a 0.5-mm arrow for H and I.

pH=5 resulted in the formation of 9 single crystals out of the 14 lanthanides (Ref. 7). The pH of the HIBA solution was chosen to mimic the conditions of column chromatographic lanthanide separation as reported in the literature (pH varies between 3 and 5, the pKa of HIBA is 3.79). Figure 1 shows the photographs of the clear rectangular plates formed. Crystallographic analysis revealed the crystals to be $Ln(HIBA)_2(H_2O)_2](NO_3)\cdot H_2O$ with Ln = La (1), Ce (2), Pr (3), Nd (4), Sm (5), Eu (6), Gd (7), Ho (10), and Er (11).

Single-crystal X-ray analysis reveals all isolated lanthanide compounds exhibit the same coordination geometry around the lanthanide atom. The thermal ellipsoid for a single unit cell for the Ln(III) is shown in Fig. 2. The Ln(III) atoms are eight-coordinate with four oxygen atoms from two chelating HIBA ligands, two oxygen atoms from two bridging HIBA ligands, and two coordinated water molecules completing the distorted dodecahedron coordination geometry. In all of the structures, HIBA adopts a monoanionic tridentate coordination with the lanthanide atom. Oxygen atoms from both the hydroxyl and the carboxylate groups chelate the Ln atom while the second carboxylate oxygen atom bridges to neighboring Ln atoms. This is in stark contrast to previously reported crystal structures of HIBA-transition metal complexes, in which the HIBA acts as a bidentate monoanion coordinating the metal atoms with two oxygen atoms from the carboxylate and hydroxyl groups. However, there are three distinct crystallographic

structures across the lanthanide series (Fig. 3 illustrates the three-dimensional packing of the three different structure types):

(a) $La(HIBA)_2(H_2O)_2](NO_3)\cdot H_2O$ (1). The unit cell contains two unique La(III) atoms; one unique nitrate (N1); and one unique lattice water (O24), which is split between the two unique lanthanum centers (one-half each). A second nitrate anion (N2) is disordered and shares partial occupancy with a second water molecule (O22 or O23).

(b) $[Ln(HIBA)_2(H_2O)_2](NO_3)\cdot H_2O$ (Ln = Ce (2), Pr (3), Nd (4), Sm (5), Eu (6), Gd (7) and Ho (10)). In contrast to 1, this structure type has only one unique Ln(III) center in the unit cell, one disordered nitrate anion, and one disordered lattice water. One oxygen atom of the nitrate is half-occupied with the lattice water (O5). The three-dimensional packing of these monoclinic complexes is different from that of complex 1 due to differences in the water-nitrate sublattice (Fig. 3). Figure 3 shows the 50% occupancy split between the disordered nitrate anion and a disordered water molecule.

(c) $Er(HIBA)_2(H_2O)_2](NO_3)\cdot H_2O$ (11). The stoichiometry and HIBA coordination mode of 11 are the same as those of Complexes 2–7 and 10. The two twinned structures are related by a two-fold symmetry. The disorder of water molecules near the nitrate is also different from the previous structures.

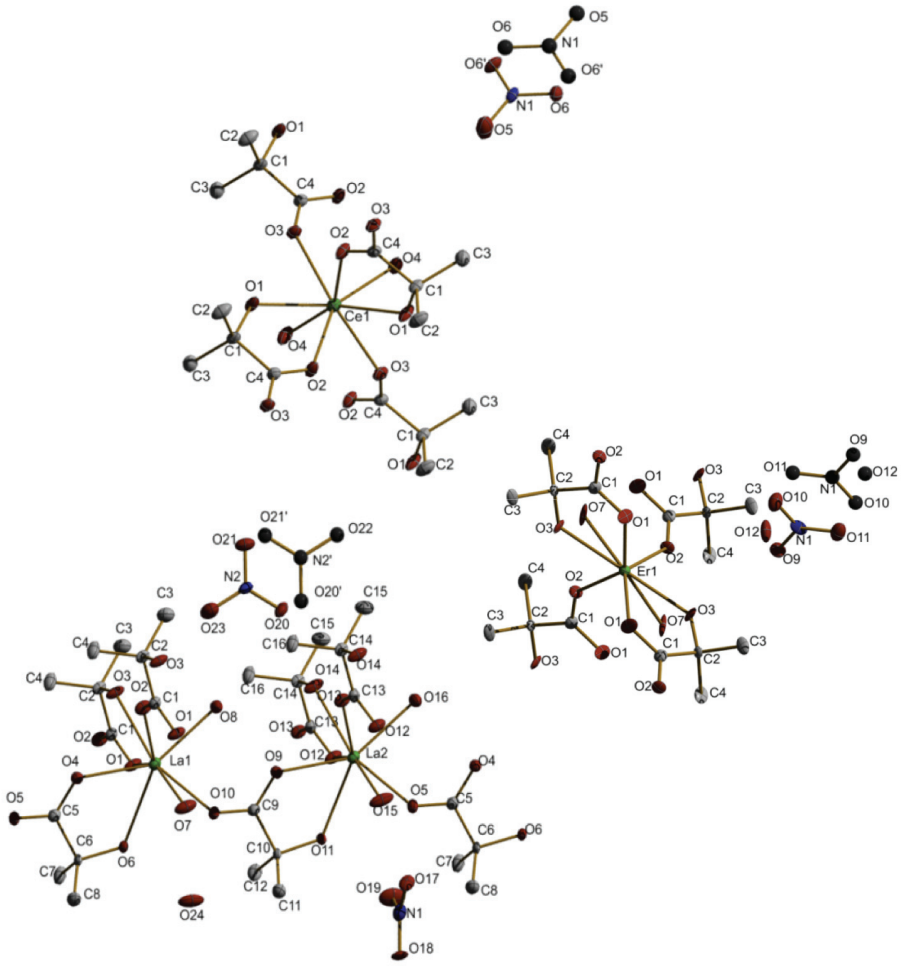

Figure 2: Thermal ellipsoids (50% probability) of $[Ln(HIBA)_2(H_2O)_2](NO_3)\cdot H_2O$ where Ln = La (left), Ce (middle) and Er (right). The hydrogen atoms have been removed for clarity. The disordered nitrates are shown as black balls.

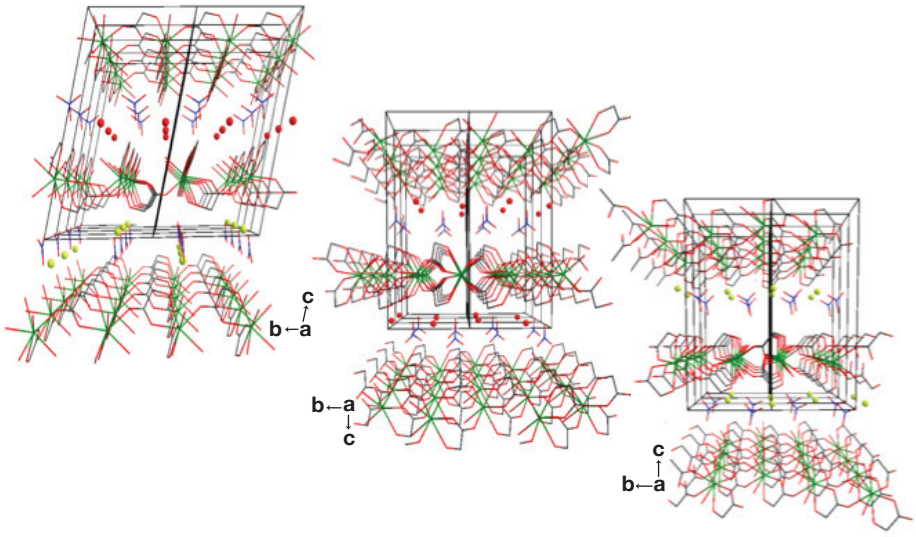

Figure 3: Three-dimensional packing of $[Ln(HIBA)_2(H_2O)_2](NO_3)\cdot H_2O$ (Ln = La, left; Ce, middle; Er, right) viewed along a axis, Ln, green; C, gray; O, red; disordered water molecule, red balls; ordered lattice water molecules, light-green balls. The hydrogen atoms and methyl groups on HIBA are omitted for clarity.

While the nitrate anions are still disordered across and inversion center, the water molecule (O12) occupies a distinct crystallographic site within the unit cell.

We analyzed powder X-ray diffraction (PXRD) on the complexes across the whole lanthanide series. For Tm, Yb, and Lu complexes, only powder precipitates were formed over the period of this study. PXRD analysis of complexes 1–7 and 10 shows excellent agreement between simulated and measured patterns. However, additional Bragg reflections can be observed in the experimental patterns of the heavy lanthanides Er–Lu that cannot be explained using the simulated pattern of the single-crystal structure determined for 11 alone. The additional Bragg reflections match very well those reflections representing compounds 1–10; thus, erbium represents a transition point in the lanthanide series with a break in the crystal structure. Under our experimental conditions the bulk precipitate is likely coprecipitating as a mixture of the two structure types. Consequently, the PXRD data is consistent with formation of $[Ln(HIBA)_2(H_2O)_2](NO_3)\cdot H_2O$ across the whole lanthanide series with three different structure types found for La, Ce–Ho, and Er–Lu.

The solid-state Raman spectra for all of the complexes are very similar because the coordination modes of HIBA are the same across the lanthanide series. After complexation, the ν(C=O) band in the free ligand is shifted to lower frequency consistent with a longer C=O bond length than in the free ligand. The higher frequency shifts of the δ(C-O) bands are also consistent with the shorter C-O bond length. The Raman band of the hydroxyl ν(C-O) mode shifted to lower frequency compared with the hydroxyl ν(C-O) stretching in free HIBA. The red shift of the hydroxyl ν(C-O) band can also be explained by the coordination of the hydroxyl oxygen atom, which results in an elongation of the $C1\text{-}O1_{hydroxyl}$ bond.

Samples of $[Ln(HIBA)_2(H_2O)_2](NO_3)\cdot H_2O$ (Ln = Pr (3), Nd (4), Sm (5), Eu (6), Dy (9), Ho (10), and Er (11)) were characterized by solid-state diffuse reflectance spectroscopy and by UV-vis-NIR spectroscopy after dissolution in water. For the solution UV-vis-NIR spectra the molar

absorptivities show general agreement with the characteristic *f-f* transitions for the Ln^{3+}(aq) ion absorbance in diluted acid. The complexation of the Ln(III) ions with HIBA results in only very small shifts of the most prominent absorbances compared with the aquo ion. Both relative intensity ratios and peak positions in the solution state UV-vis-NIR spectra and their solid state UV-vis-NIR diffuse reflectance spectra match well, suggesting similar coordination environments around the lanthanide in solution and solid state.

We also used ^{13}C-NMR spectroscopy to explore the speciation in solution. Uncomplexed HIBA at pH 5 shows three ^{13}C-NMR signals at 73.07 ppm for the hydroxyl carbon, 26.06 ppm for the methyl carbons, and 183.32 ppm for the carboxyl carbon. All coordinated HIBA ligands in the HIBA-Ln(III) solution complex are equivalent and display the same ^{13}C-NMR features shifted from those of the free ligand. When HIBA is chelating a metal ion, the carbon atoms of the COOH and C(OH) groups are deshielded, illustrated as coordination-induced shifts, $\Delta\delta$. The $\Delta\delta$ values are 3.5 (C(OH)) and 0.7 ppm (COOH) for the La(III) solution complex and 4.2 (C(OH)) and 0.4 ppm (COOH) for the Lu(III) solution complex indicate that both the hydroxyl and the carboxyl groups of the HIBA ligand are coordinated with the Ln(III) groups. As expected, the $\Delta\delta$ values for the methyl carbons are smaller than observed for the binding functional groups. Notably, the chemical shifts for the La(III) complex in the supernatant during crystallization is nearly identical to those observed after dissolving the La(III) crystal in water at pH 5, indicating that only one solution complex exists at the conditions investigated.

In summary, we investigated the solid-state and solution-state coordination chemistry of HIBA with lanthanides, which furthers our fundamental scientific understanding of the structure and bonding of lanthanide complexes with HIBA under conditions most relevant to physiological processes and recycling of used nuclear fuel.

References:

1. *Silva, J. Inorg. Nucl. Chem. 1956, 3, 153.*
2. *K. Nash and M. Jensen in Handbook of Phys. Chem. Rare Earths, K.A. Gschneider and L. Eyring, Eds., Vol. 28, p. 311, Elsevier, New York, 2000.*
3. *L.W. Holm, G.R. Choppin, D.J. Moy, J. Inorg. Nucl. Chem. 1961, 19, 251.*
4. *W.R. Stagg and J.E. Powell, Inorg. Chem. 1964, 3, 242.*
5. *H. Deelstra and F. Verbeek, Anal. Chim. Acta, 1964, 31, 251.*
6. *F. Kin, Z. Ni, C. Xu, Wuji Huaxue Xuebao, 1994, 10, 266.*
7. *X.Y. Chen, G.S. Goff, W.C. Ewing, B.L. Scott, W. Runde, Inorg. Chem. 2012, 51, 13254.*

Relaxation of Radiation Damage in Plutonium

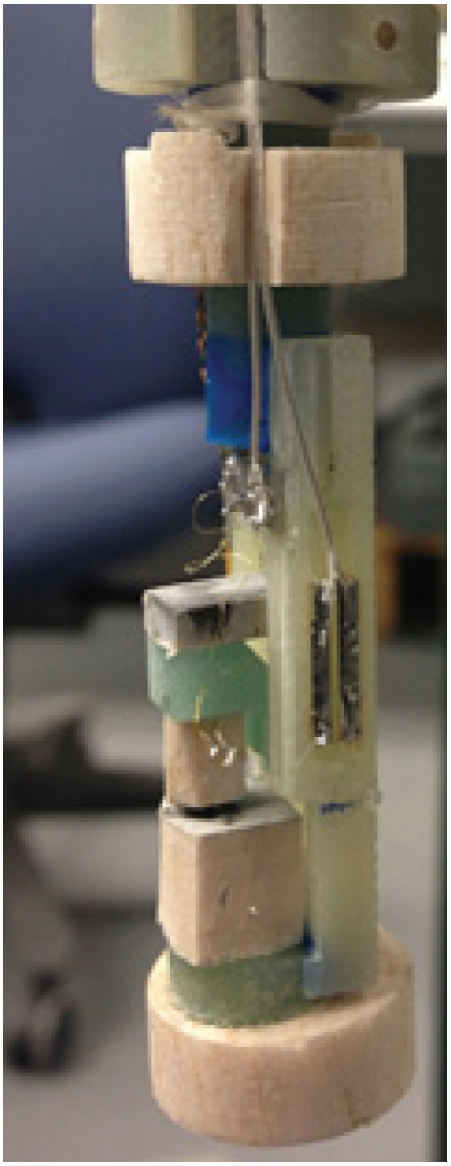

Arkady Shehkter

Arkady Shehkter is a current Seaborg postdoc in Materials Physics and Applications Division, Condensed Matter and Magnet Science (MPA-CMSS). His area of interest is phonon-driven electron localization in δ plutonium. Albert Migliori is his mentor.

Figure 1: A resonant ultrasound assembly used to measure changes in thermodynamic properties in modern condensed matter systems, such as high temperature superconducting cuprates. Our measurements on plutonium use an ultrasound probe of similar design.

Plutonium has no future—all of its isotopes decay over time, albeit that time is quite long, about 25,000 years for the isotope 239Pu. About a billion atoms decay every second in 1 gram of plutonium, such that every two atoms that decay within 1 second of each other are on average 10,000 lattice sites apart. This decay does not just introduce a single atomic defect, but introduces macroscopic changes in properties of the crystal. These arise not only from the accumulation of decay products such as 4He, uranium, but importantly, from the enormous kinetic energy of the decay products. This energy is dissipated by displacing a large number of atoms from their ideal lattice positions. The defects in a crystal lattice (so-called radiation damage) come in (Frenkel) pairs: one, for the plutonium atom in between lattice sites (interstitial) and one, for the missing atom in plutonium lattice (vacancy). At finite temperature the vacancies and interstitials are diffusing slowly such that once in a while they coincide, annihilating to repair some of the radiation damage. These events continue indefinitely: the macroscopic equilibrium of crystalline plutonium is dynamic in nature. Unlike the universal decay of plutonium atoms, the character of the equilibrium state of the crystal and the slow rate at which this equilibrium is approached are strongly dependent on temperature and the history of a crystal.

Plutonium (as any other) lattice is softening when more crystal bonds are damaged by vacancies and interstitials. Therefore, elastic stiffness, if measured with enough accuracy, is a reliable measure of the instantaneous state of the damaged crystal lattice. Using resonant ultrasound spectroscopy (Fig. 1) we measured the evolution of the elastic properties of a cylindrical

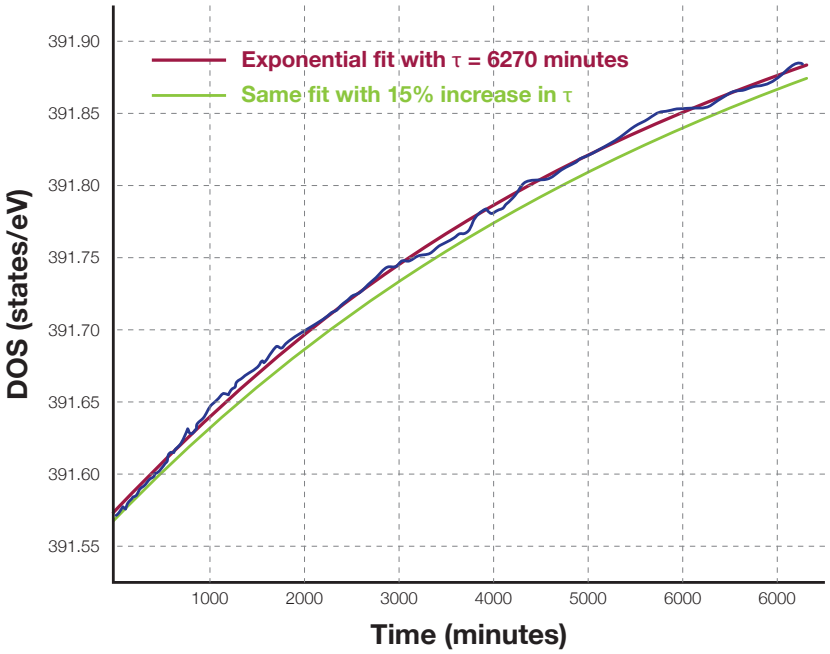

Figure 2: Exponential fit to the time dependence of the shear resonance of Pu 1.7at% Ga at 320 K. The time constant is about 4.4 days (with about 10% error bar) and the total increase in stiffness over a period of about 5 days 0.1%, indicating a reduction in defect density on rising temperature. Although defects induce softening, the effect is generally weak on the bulk modulus. Thus a 0.1% change in bulk modulus may reflect a substantial change in defect density. The material was stabilized at 300 K for some time before the measurements began. The temperature has been subsequently increased abruptly (in about a half an hour) to 320 K and has been controlled at this value over a period of about a week. The temperature stability was about 40 mK.

plutonium sample in real time (every 10–50 seconds) with precision of order 1 part in $10^{\wedge 7}$ (Fig. 2).

The defect density in plutonium is determined by two competing factors. The first is the ordinary thermal activation of vacancy loops with increasing temperature. The second is the introduction and equilibration of Frenkel pairs generated by radioactive decay. Thermally induced diffusion of radiation-induced interstitials and vacancies is responsible for the changes in elastic properties over a few days. Thus the time evolution of the elastic properties over this period gives a direct indication of the character and rates of diffusion of the defects. Although microscopically the diffusion rates are only determined by temperature, they might also report on the microstructure history of the crystal via effects such as pinning.

Continuing these measurements will clarify the physical phenomena that control the density and spatial distribution of Frenkel pairs as well as the character of their diffusion. It is essential to improve the accuracy and control of the temperature over extended periods of time. In particular, our results suggest that the temperature history of a plutonium sample must be controlled for many days before a dynamic or shock measurement is made to ensure consistency in defect density conditions. To begin understanding the dynamics of defects in plutonium crystal, we need a quantitative understanding of the effects of Frenkel pair density on the elastic properties of crystal.

Acknowledgement

I would like to thank Albert Migliori for letting me follow him in the complex field of physics of actinide materials and for his help in writing this article. I thank Brad Ramshaw for being essential part of this experimental project and Ross McDonald and Kim Modic for critical reading of the manuscript.

Controlling Actinide Extractions through Covalency

Background and Significance

One of the central chemical challenges facing the development of advanced fuel cycles involves removing trivalent minor actinides (Am, Cm) from trivalent lanthanides present in spent nuclear fuel. The separation of these 4*f* and 5*f* elements is particularly difficult because they share many chemical properties. For example, their reactivity is dominated by extreme oxophilicity and the common trivalent oxidation state. Despite these similarities, a number of "soft-donor" ligands have been identified that selectively extract minor actinides, albeit with varying degrees of success (Scheme 1).[1-3] Often, it is not obvious why one particular "soft-donor" extractant outperforms another. This researcher directly addresses the problem and presents an alternative strategy for identifying key electronic features associated with the extractant that may facilitate selective binding of actinides over lanthanides. Overall, the work is focused on using the insight generated from the electronic structure and covalency studies in the design of new extractants that are more tailored for application in advanced fuel cycles.

Results and Discussion

In this study, we have applied two techniques routinely used to evaluate orbital mixing and electronic structure in inorganic and bioinorganic systems to the field of actinide/lanthanide separations science, namely ligand K-edge X-ray absorption spectroscopy (XAS) and time-dependent density functional theory (TDDFT).[4] The research focused on providing insight into how the ancillary groups attached to phosphorus affect the electronic structure and bonding in dithiophosphinate extractants, and direct their ability to extract minor actinides (like Am and Cm) from lanthanides. Solid-state XAS analyses and DFT calculations suggest the *ortho* substituent in C_2-$S_2P(o\text{-}CF_3C_6H_4)_2^{1-}$ inhibits rotation of the aryl groups into C_{2v} symmetry,[5] thereby holding the $S_2P(o\text{-}CF_3C_6H_4)_2^{1-}$ ion in an "entatic state," or geometric configuration that appears electronically poised for higher actinide binding selectivity (Figure 1-left).[6]

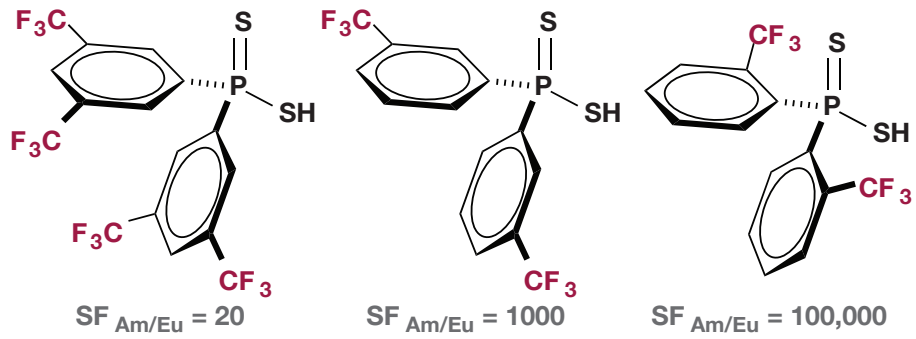

Angela Olson

Angela Olson is a current Seaborg postdoc. Her area of interest is investigation of covalency in dithiophosphinate actinide extractants using S K-edge X-ray absorption spectroscopy. Her mentor is Stosh Kozimor, C-IIAC.

Scheme 1: What makes $S_2P(o\text{-}CF_3C_6H_4)_2^{1-}$ superior?

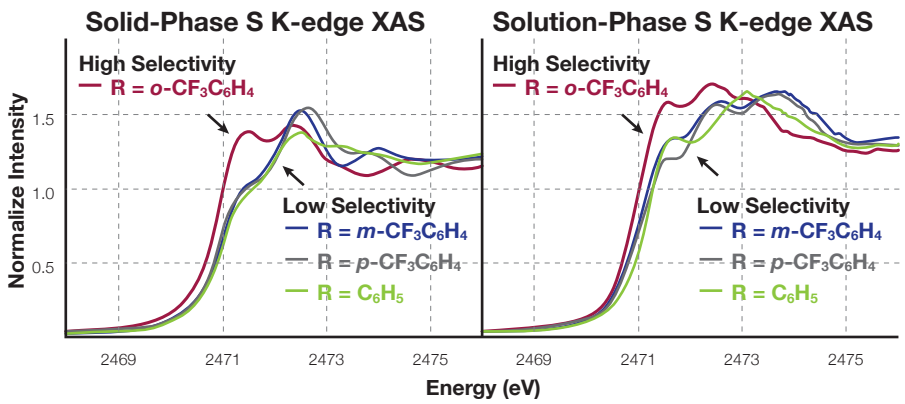

Figure 1. The unique electronic structure of $S_2P(o\text{-}CF_3C_6H_4)_2^{1-}$ is evident by S K-edge XAS analysis in both the solid- (left)[4] and solution-phase.

While the S K-edge XAS measurements collected on analytes in the solid state demonstrate a clear correlation between electronic structure and the ability of certain dithiophosphinate extractants to remove minor actinides from lanthanide contaminants present in spent nuclear fuel, an additional challenge lies in identifying if these conclusions are relevant once the extractants are dissolved. For example, in solution (where actinide/lanthanide extractions occur), the arene rings in $S_2P(o\text{-}CF_3C_6H_4)_2^{1-}$ may be able to freely rotate away from the actinide binding entatic state defined above. To evaluate the validity of the solid-state conclusions on solution-phase extractant behavior, we have developed capability for conducting analogous solution-phase S K-edge XAS measurements.

Many technical obstacles exist for solution-phase S K-edge XAS that are not of concern for analogous solid-state studies. Briefly, because the S K-edge (2472 eV) is at relatively low energy, the incident X-ray radiation and subsequent sample fluorescence is easily attenuated by windows required to contain the solution within a sample cell. Additionally, sample degradation caused by radiolysis can be far more pronounced in solution than in the solid state. Recent advances in beam line instrumentation at synchrotron facilities suggest that these challenges can be overcome at the S K-edge. As testament, although solution S K-edge XAS measurements are rare, a number of S K-edge XAS studies of analytes in aqueous and organic solutions have recently been reported.[7-12] For our purposes, we have overcome these obstacles using the S K-edge XAS sample cell shown in Fig. 2. This cell is equipped with a peristaltic pump for continuously flowing analyte solution through the beam, and is connected to a Schlenk line, so that samples can be analyzed with rigorous exclusion of air and moisture. Combined, the continuous flow and air-sensitive capabilities decreased the amount of unwanted sample degradation (due to radiolysis) during the XAS solutions measurements.

Following the design of the solution-phase S K-edge XAS cell, measurements on dithiophosphinate extractant ligands commenced (Fig. 1-right). The solution-phase XAS study provided data consistent with measurements acquired in the solid state. For example, direct comparisons of the $S_2PR_2^{1-}$ solid- and solution-state S K-edge XAS data (Fig. 1) show similar features in the low energy side of the pre-edge region (<2473 eV), albeit with subtle differences in peak intensity. These differences were likely due to

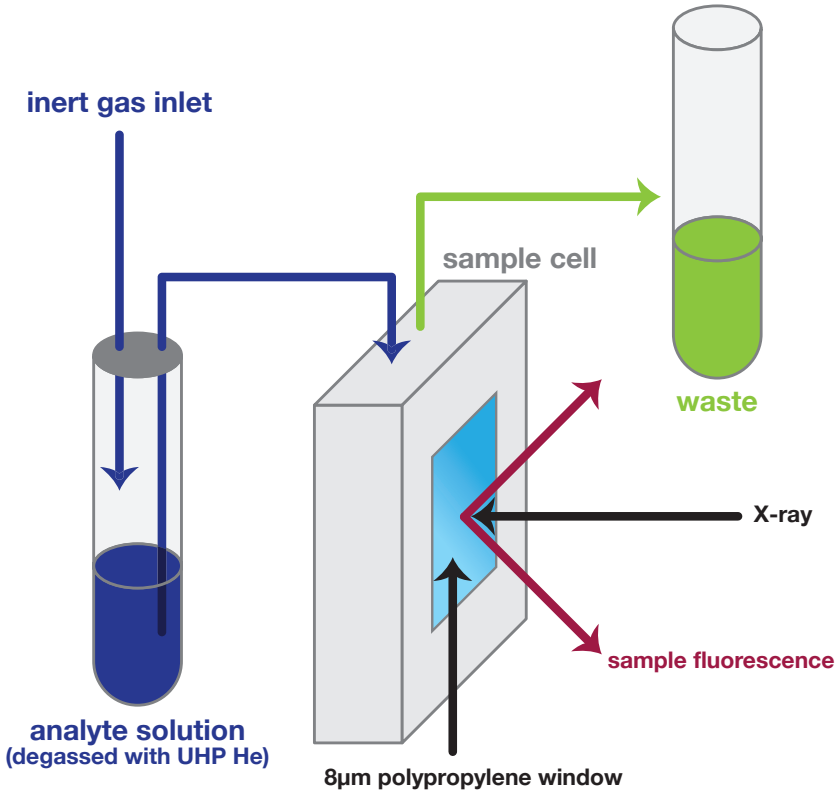

Figure 2: Solution-phase S K-edge XAS capabilities were established using a specially engineered sample flow cell.

additional degrees of freedom available to the analyte in solution. Despite these dynamic conditions, the data suggest that the *ortho*-CF_3 substituent in $S_2P(o\text{-}CF_3C_6H_4)_2^{1-}$ still inhibits rotation of the aryl groups, thereby holding the $S_2P(o\text{-}CF_3C_6H_4)_2^{1-}$ in its unique actinide binding entatic state. Future work is focused on using the solution-phase S K-edge XAS capability to evaluate how metal–sulfur orbital mixing influences actinide/lanthanide separations under dynamic liquid/liquid extraction conditions.

Having fully characterized the inductive effects of the ancillary arene groups on P–S bonding, our efforts have now shifted to studies on $S_2PR_2^{1-}$ interactions with actinide and lanthanide elements. This work uniquely focuses on quantifying the relative contributions of 6d vs 5*f* orbitals in covalent M–S bonding. Hence, a series of f-element $M(S_2PPh_2)_4^{x-}$ (M = Nd, x = 1; M = U, Np, x = 0; Fig. 3) complexes have been analyzed in the solid state using S K-edge XAS at the INE beam line for actinide research at Angstroemquelle Karlsruhe (ANKA) (Fig. 4). Preliminary peak assignments in these spectra were made based on a systematic study of d-block transition metal–, lanthanide–, and actinide–dithiophosphinate complexes by S K-edge XAS and TDDFT. The prominent feature near 2472 eV has been tentatively assigned to transitions to orbitals resulting from the S 3p orbitals mixing with the metal d-orbitals. As expected, these transitions are observed at low energy for the 5d orbitals of Nd and move to higher energy for the 6d orbitals of U and Np. In addition, the intensity for the pre-edge features (which is directly related to the amount of metal-ligand orbital mixing) systematically increases, such that Nd < U < Np. In addition to Np showing the largest amount of M 6d and S 3p orbital mixing (or covalency), the

Acknowledgement

The research described here has been carried out by a multidisciplinary team that spans LANL and INL expertise in radiochemistry, synthesis, theory, and spectroscopy. Members of the team include Angela C. Olson, Jason M. Keith, Enrique R. Batista, Kevin S. Boland, Scott R. Daly, David L. Clark, Andrew J. Gaunt, Gordon D. Jarvinen, Stosh A. Kozimor, Molly M. MacInnes, Richard L. Martin, and Brian L Scott. Members of the INL team include John R. Klaehn and Dean R. Peterman. This work has been supported under the Heavy Element Chemistry Program at LANL by the Division of Chemical Sciences, Geosciences, and Biosciences, Office of Basic Energy Sciences and by the U.S. Department of Energy, Office of Nuclear Energy (Fuel Cycle R&D Program). Portions of this research were carried out at the Stanford Synchrotron Radiation Lightsource (SSRL), a Directorate of SLAC National Accelerator Laboratory and an Office of Science User Facility operated for the U.S. Department of Energy Office of Science by Stanford University. We acknowledge the Synchrotron Light Source Angstroemquelle Karlsruhe (ANKA) for provision of instruments at its beamlines and we thank Tonya Vitova, Kathy Dardenne, Jörg Rothe, and Melissa Denecke for assistance in using the INE-Beamline. Parts of this work were supported at LANL by the Glenn T. Seaborg Institute Postdoctoral Fellowships (Olson, Daly) and a Director's Postdoctoral Fellowship (Keith).

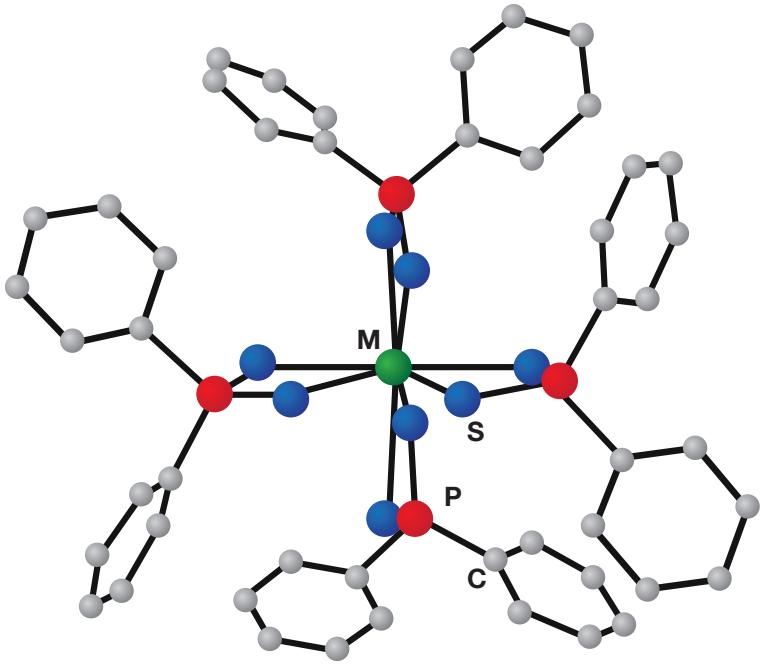

Figure 3: $M(S_2PPh_2)_4^{x-}$ (M = Nd, x = 1; M = U, Np, x = 0) were synthesized and studied using ligand K-edge XAS.

Np spectrum is unique in that a small pre-edge feature near 2470 eV has emerged. Based on previously established d- and f-orbital energy trends, this lower-energy feature is likely associated with Np 5*f*-orbital mixing with the S 3p orbitals, providing the first unambiguous experimental evidence for actinide-sulfur covalent bonding.[13,14]

Summary

The term "soft-donor" extractant is used collectively to refer to extractants that exhibit selectivity for minor actinides. The term arises primarily from empirical data obtained from the screening of organic extractants in minor actinide extraction studies. Within the context of hard-soft acid-base theory, the vast majority of extractants that exhibit selectivity for minor actinides contain donor atoms that are considered to be softer bases than oxygen (N, S, Cl). Hence, as the name implies, it is assumed that ligand softness is important for directing effective separations. While there are remarkable trends in minor actinide selectivity in comparisons with otherwise identical ligands containing donor atoms of varying softness [e.g., $S_2P(o\text{-}CF_3C_6H_4)_2^{1-}$ (SF = 100,000) vs $O_2P(o\text{-}CF_3C_6H_4)_2^{1-}$ (SF = 0.01)], it is not clear whether the trend relating ligand softness and selectivity holds in comparisons among a series of ligands containing identical soft-donor atoms. In this study, we have demonstrated that ligand K-edge XAS and TDDFT can be used to quantify electronic structure variations that relate to ligand softness, and we have shown that the special electronic properties observed for $S_2P(o\text{-}CF_3C_6H_4)_2^{1-}$ correlate with its exceptionally high minor actinide selectivity. Additionally, we have demonstrated that conclusions based on solid-state analyses are also relevant in solution on the time-scale of our S K-edge XAS measurements. Overall, results from both the solid- and solution-phase measurements provide a foundation for distinguishing S K-edge XAS transitions attributed to P–S ligand bonding from transitions

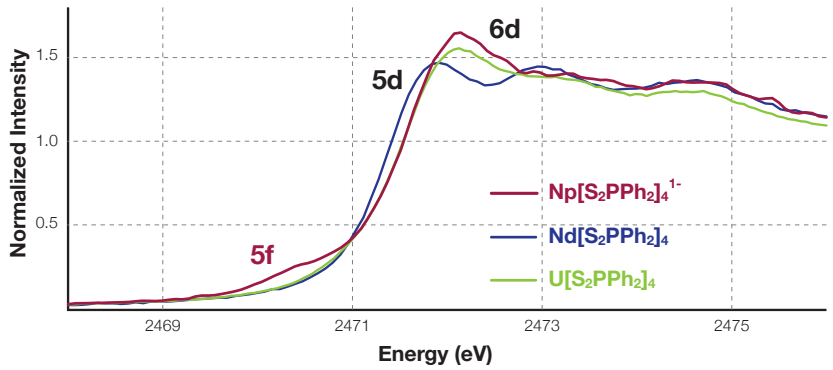

Figure 4: S K-edge XAS analysis of $M(S_2PPh_2)_4^{x-}$ reveals unambiguous evidence for covalent bonding between Np 5f and S 3p orbitals.

associated with metal-sulfur interactions, which is essential for the analyses of $M(S_2PR_2)_x^{(3-x)}$ complexes (M = trivalent minor actinide or lanthanide) that are currently in progress. We anticipate that these S K-edge XAS and TDDFT results will provide valuable insight into structure-to-function relationships in dithiophosphinate extractants, which can be used for future innovation in minor actinide extraction chemistry to support the development of advanced nuclear fuel cycles.

Further Reading:

1. *Xu, Q.; Wu, J.; Chang, Y.; Zhang, L.; Yang, Y., "Extraction of Am (III) and lanthanides (III) with organo dithiophosphinic acids", Radiochim. Acta* **2008**, *96, 771–779.*
2. *Klaehn, J.R.; Peterman, D R.; Harrup, M.K.; Tillotson, R.D.; Luther, T.A.; Law, J.D.; Daniels, L. M., "Synthesis of symmetric dithiophosphinic acids for "minor actinide" extraction", Inorg. Chim. Acta 2008, 361, 2522–2532.*
3. *Peterman, D.R.; Greenhalgh, M.R.; Tillotson, R.D.; Klaehn, J.R.; Harrup, M.K.; Luther, T.A.; Law, J.D. "Selective extraction of minor actinides from acidic media using symmetric and asymmetric dithiophosphinic acids", Sep. Sci. Technol. 2010, 45, 1711–1717.*
4. *Solomon, E.I.; Hedman, B.; Hodgson, K.O.; Dey, A.; Szilagyi, R.K., "Ligand K-edge X-ray absorption spectroscopy: covalency of ligand–metal bonds",. Coord. Chem. Rev. 2005, 249, 97–129.*
5. *Daly, S.R.; Keith, J.M.; Batista, E.R.; Boland, K.S.; Clark, D.L.; Kozimor, S.A.; Martin, R.L. J. Am. Chem. Soc. 2012, 134, 14408–14422.*
6. *Vallee, B.L.; Williams, R.J, "Metalloenzymes: the entatic nature of their active sites", Proc. Natl. Acad. Sci. U.S.A. 1968, 59, 498–505.*
7. *Sarangi, R.; Frank, P.; Benfatto, M.; Morante, S.; Minicozzi, V.; Hedman, B.; Hodgson, K.O., "The x-ray absorption spectroscopy model of solvation about sulfur in aqueous L-cysteine", J. Chem. Phys. 2012, 137, 205103.*
8. *Damian, E.; Jalilehvand, F.; Abbasi, A.; Pettersson, L. G. M.; Sandström, M.; Szargan, R., "Sulfur K-edge x-ray absorption spectra for dimethyl sulfoxide in the solvated thallium(III), indium(III), gallium(III) and aluminum(III) ions", Physica Scripta 2005, 1077.*
9. *Frank, P.; Hedman, B.; Hodgson, K. O., Sulfur Allocation and Vanadium–Sulfate Interactions in Whole Blood Cells from the Tunicate Ascidia ceratodes, Investigated Using X-ray Absorption Spectroscopy", Inorg. Chem. 1999, 38, 260–270.*
10. *Frank, P.; Hedman, B.; Carlson, R.M. K.; Hodgson, K.O., "Interaction of Vanadium and Sulfate in Blood Cells from the Tunicate Ascidia ceratodes: Observations Using X-ray Absorption Edge Structure and EPR Spectroscopies", Inorg. Chem. 1994, 33, 3794–3803.*
11. *Shadle, S.E.; Hedman, B.; Hodgson, K.O.; Solomon, E.I., "Ligand K-Edge X-Ray Absorption Spectroscopic Studies: Metal-Ligand Covalency in a Series of Transition Metal Tetrachlorides", J. Am. Chem. Soc. 1995, 117, 2259–2272.*
12. *Frank, P.; Hedman, B.; Carlson, R. M.K.; Tyson, T.A.; Roe, A.L.; Hodgson, K.O., "A large reservoir of sulfate and sulfonate resides within plasma cells from Ascidia ceratodes, revealed by X-ray absorption near-edge structure spectroscopy", Biochemistry 1987, 26, 4975–4979.*
13. *Minasian, S. G.; Boland, K. S.; Feller, R. K.; Gaunt, A. J.; Kozimor, S. A.; May, I.; Reilly, S. D.; Scott, B. L.; Shuh, D. K. Inorg. Chem. 2012, 51, 5728–5736.*
14. *Kozimor, S.A.; Yang, P.; Batista, E.R.; Boland, K.S.; Burns, C.J.; Clark, D.L.; Conradson, S.D.; Martin, R.L.; Wilkerson, M.P.; Wolfsberg, L.E., Trends in covalency for d- and f-element metallocene dichlorides identified using chlorine K-edge X-ray absorption spectroscopy and time-dependent density functional theory", J. Am. Chem. Soc. 2009, 131, 12125–12136.*

Alison Pugmire

Alison Pugmiree was a Seaborg Fellow from February 2008--November 2010. Her area of interest was spectroscopic studies of actinide systems, with mentor Iain May of C-IIAC. She is now a staff member in Materials Science and Technology Division, Nuclear Materials Science Group (MST-16).

Spectroscopic Analysis of Actinyl Systems

The coordination chemistry of the actinides continues to be an area of intense research, particularly for environmental remediation purposes, nuclear waste management, and nuclear fuel separation technologies. A detailed understanding of the structure and bonding properties of the actinyls is essential to successfully developing and applying these technologies. We investigated a series of actinyls {$U(VI)O_2^{2+}$, $Np(V)O_2^{+}$, $Np(VI)O_2^{2+}$, $Pu(VI)O_2^{2+}$} coordinated to heteropolyoxometalate (POM) ligands. These early transition metal-oxygen clusters are particularly useful because they readily coordinate a range of actinyls {$An(V)O_2^{+}$ and $An(VI)O_2^{2+}$ where An = U, Np, Pu, Am} and form structurally diverse complexes with distinct spectral signatures (absorbance and luminescence). Previous work in 2007 at the University of Manchester (Manchester, UK) by Stephen Faulkner (Manchester) and Los Alamos researchers Iain May (C-IIAC) and Roy Copping (C-IIAC) revealed POM coordination enhances {$Np(VI)O_2^{2+}$} luminescence. In subsequent work at Los Alamos in 2009, May, Copping, Andrew Gaunt and Sean Reilly of C-IIAC discovered these POM ligands stabilize *three* Pu(VI) actinyls. While intriguing, these $5f^1$ and $5f^2$ systems were spectroscopically complex and experimentally limited (material availability, high radioactivity). The electronically simpler ($5f^0$) and less radioactive uranyl analogs were therefore chosen to conduct a more expansive spectroscopic investigation.

Our initial focus began with the $[(X)_2(UO_2)_2(A\text{-alpha-}PW_9O_{34})_2]^{12-}$ (where X = Na^+, NH_4^+, K^+) series (Fig. 1) first studied by Kim and Pope in 1999.[1] The relative ease of synthesis and their stability in solution (particularly aqueous solution) made these complexes ideal for this work. The '$[A\text{-}PW_9O_{34}]^{9-}$' POM in Fig. 1 forms a semi-cage-like structure, encapsulating the actinyl above and below the actinyl equatorial plane. Each uranyl $\{UO_2\}^{2+}$ moiety ($[A\text{-}PW_9O_{34}]^{9-}$, Fig. 1) is bound to five terminal

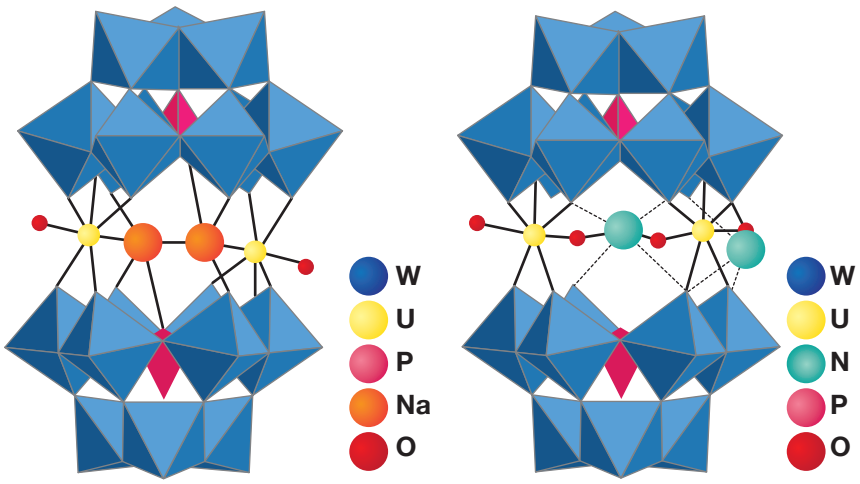

Figure 1: Structural representation of the uranyl polyoxometalate clusters, $[X_2(UO_2)_2(PW_9O_{34})_2]^{12-}$, X=$Na^+$ (left), NH_4^+ and K^+ (right).

POM oxygens (represented by a polyhedron edge) via the uranyl equatorial oxygens (O_{eq}). The internal uranyl axial oxygen (O_{ax}) is bound to a cation in the center of the complex. Changes to this structural motif were then varied and included changing: 1) the internal cation (Na^+, NH_4^+, or K^+ and represented by the orange or aqua sphere in Fig. 1); 2) the ligand isomer (the rotational orientation of the POM relative to the uranyls), and 3) the POM heteroatom ($[XW_9O_{34}]^{9-/10-}$, where X = P, Ge, Si and is represented by a pink polyhedron in Fig. 1). One interesting note first observed by Kim and Pope is the alteration of the structure when the internal cation is varied. When sodium is the cation, two sodium atoms are incorporated in the center of the structure (Fig. 1, left). However, when ammonium or potassium are the cations, only one atom is coordinated to both uranyls (Fig. 1, right).

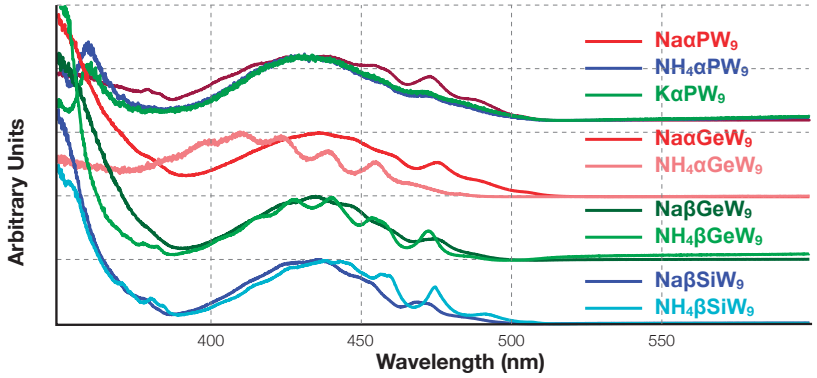

Figure 2: Diffuse reflectance (solid state absorption) of $[X_2(UO_2)_2(y\text{-}ZW_9O_{34})_2]^{12-/14-}$, where X = Na, NH_4, K, y = α or β and Z = P, Ge, Si.

Our previous work on actinyl-POM systems indicated these variations in structure would produce changes in the spectroscopic signatures. This was indeed the case for several of the uranyl-POMs studied here. Absorption spectra were obtained for all complexes in solution (data not shown) and the solid state (Fig. 2). Below 350 nm, the sharp increase in the absorption coefficient corresponds to charge transfer bands; the visible region (350 nm–525 nm) corresponds to uranyl $\{UO_2^{2+}\}$ transitions. The uranyl transitions are formally forbidden and gain intensity through vibronic coupling. This vibronic coupling manifests itself as distinct peaks, or "fine structure," superimposed on the main transition and is typical of uranyl absorption and emission. All complexes studied here display similar absorption maxima (ca. 435 nm, Fig. 3) with one notable exception: NH_4^+-[A-α-GeW_9O_{34}]. In this complex, germanium substitutes phosphorus as the POM heteroatom, and the absorption spectrum shows a maximum that is shifted to lower wavelength (ca. 410 nm). Such 'shifts' in the maxima of the uranyl fine structure were previously seen (by Görller-Walrand and De Jaegere in 1972, for instance) and are attributed to differences in the geometry (symmetry) of the uranyl coordination environment.[2] Subsequent structural characterization of this complex by single crystal X-ray diffraction revealed the bonding environment of the complex was in fact different. Instead of two uranyls sandwiched between the [A-α-$GeW_9O_{34}]^{10-}$ anions, a third $\{UO_2\}^{2+}$ cation partially a third site (40% occupancy) in the complex. Clearly, this change in structure resulted in a noticeable change in the spectroscopic signature.

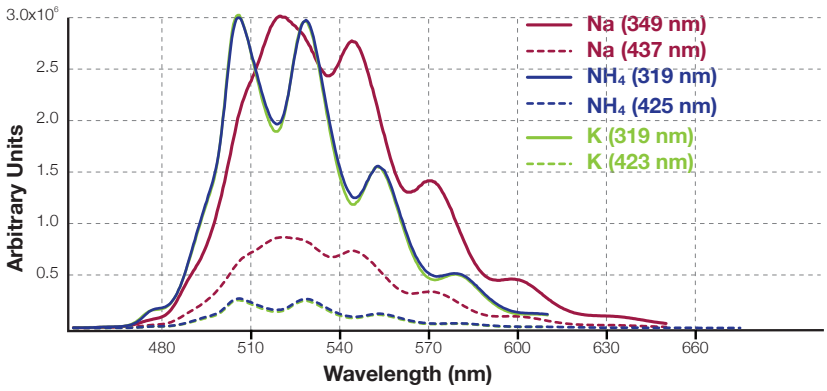

Figure 3: Room temperature solution luminescence spectra for the 'PW_9' series: $X_2(UO_2)_2(PW_9O_{34})_2]_{12}$ (X = Na, NH_4, K) after excitation from the charge transfer region (<350 nm) and uranyl region (>350 nm).

The luminescence spectra of these uranyl-POMs also produced interesting results (Fig. 3, 'PW_9' series). The emission profiles were generated by excitation of the two regions seen in the absorption spectra: 1) the charge transfer region (<350 nm), and 2) the uranyl fine structure (ca. 435 nm). Both excitation pathways resulted in spectra with well-resolved vibronic fine structure. However, accessing the more intense, charge transfer region produced more intense luminescence spectra than excitation of the uranyl region. This result correlates well with the charge transfer bands being spectroscopically allowed versus the formally forbidden uranyl region. The most significant change in the luminescence was observed when Na^+ is the counter-cation for the 'PW_9O_{34}' ligand. The emission profile shows a distinct shoulder on the first peak and indicates more than one vibronic progression exists. This result is being attributed to the structural differences in Fig. 1, where two Na^+ cations (instead of one $NH4^+$ or K^+) are incorporated in the center of the complex.

These results highlight a few of the spectroscopic changes observed when altering the POM heteroatom (P, Ge, Si) or the coordinating cation (Na^+, NH_4^+, K^+). The full breadth of this work includes solution and solid state luminescence studies, at room temperature and at 77 K, as well as a complete set of absorption and Raman data for all complexes. Overall, these uranyl-POMs highlight the effect subtle structural variations have on the spectroscopic signatures. This work has laid the foundation for understanding their origin and will be extended to other actinyl-POMs in the future.

Acknowledgement

This work was made possible by the Seaborg Institute Postdoctoral Fellows Program, of which Alison (Costello) Pugmiree was a Fellow from 2008–2010. This postdoctoral fellowship was instrumental in providing her with the opportunity to work with world-class actinide scientists while strengthening her own expertise in the area. She was hired as a technical staff member in 2010 in MST-16 studying plutonium surface science and corrosion. Recently, Alison was granted an LDRD Early Career Research award studying plutonium oxidation and corrosion using a variety of surface science and spectroscopic techniques. Additional support for this work was received through the Office of Basic Energy Sciences (Heavy Element Chemistry Program) and the Los Alamos National Laboratory Directed Research and Development (LDRD) program.

Further Reading:

1. K-C Kim and M.T. Pope, "Cation-Directed Structure Changes in Polyoxometalate Chemistry. Equilibria between Isomers of Bis (9-tungstophosphatodioxouranate(VI)) Complexes", J. Am. Chem. Soc., 1999, 121 (37), 8512–8517.
2. C. Görller-Walrand, S. De Jaegere, "Correlation between the vibronic spectra of the uranyl ion and the geometry of its coordination", Spectrochimica Acta Part A: Molecular Spectroscopy, Volume 28, Issue 2, 1972, 257–268

Understanding Correlated Electron Behavior in Lanthanide- and Actinide-Containing Intermetallics:

Synthesis, Structure, and Physical Properties

The nature of correlated electron behavior in lanthanide- and actinide-containing materials is one of the ever-evolving fields of study for condensed matter physicists. Specifically, the 4*f* and 5*f* electrons can yield a variety of exotic properties including heavy fermion behavior, superconductivity, and magnetism. It has also been demonstrated that this behavior can happen following changes in temperature, pressure, magnetic field, chemical substitution. Most of the physical property measurements done on these materials take place at low temperatures. Under these conditions, we can freeze out the phonon contributions, thereby making it easier to detect and shed light on this correlated electron behavior.

Research on understanding the complex nature of the 4*f* and 5*f* electrons addresses many of the key objectives outlined in the *2013 Integrated Plutonium Science and Research Strategy* published by Los Alamos National Laboratory (LANL) and Lawrence Livermore National Laboratory (LLNL).[1] The objectives are to increase understanding of the electronic ground states of actinides, phase stability, aging effects, and the dynamic behavior of actinides when subjected to extreme conditions such as pressure, temperature, time, and phase space. Making the connection between the 4*f* and 5*f* electrons through the study of isostructural lanthanide- and actinide-based intermetallics will enable establishment of an equation of state for these materials, demonstrating how the 5*f* electrons behave in extreme conditions.

Both the lanthanides and actinides have many electronic states that can span the extremes from localized to delocalized (itinerant) behavior. Probing the complex physics therefore partly depends on the study of a number of intermetallics that display this behavior as well as systems not so clearly defined by either extreme. We have studied a number of intermetallic systems that fit exactly into this scheme of research. We have reported a few cerium (Ce), ytterbium (Yb), and uranium (U)-based materials that offer a variety of physical properties, some of which we explain in more detail. Others include but are not limited to the study of a new heavy fermion Ce-based compound with the chemical formula $CePd_{1+x}Al_{6-x}$ (x = 0.5), a new rhombohedral Yb intermetallic $YbNi_3Al_{9.23}$ that exhibits a very high ordering temperature for Yb with its 4*f* electrons being fairly localized, and an interesting tetragonal U-containing compound with the formula UIr_4Al_{15}.[2,3,4] Electrical resistivity under hydrostatic pressure shows that

Paul H. Tobash

Paul Tobash was a Seaborg postdoc from March 2009–March 2011. His area of study was synthesis of heavy fermion superconductors through exploitation of atomic-level building blocks and crystal chemistry. His mentor was Eric Bauer, of the LANL Condensed Matter and Magnet Science Group (MPA-CMMS). Paul converted to a LANL staff member in MPA-CMMS in 2011.

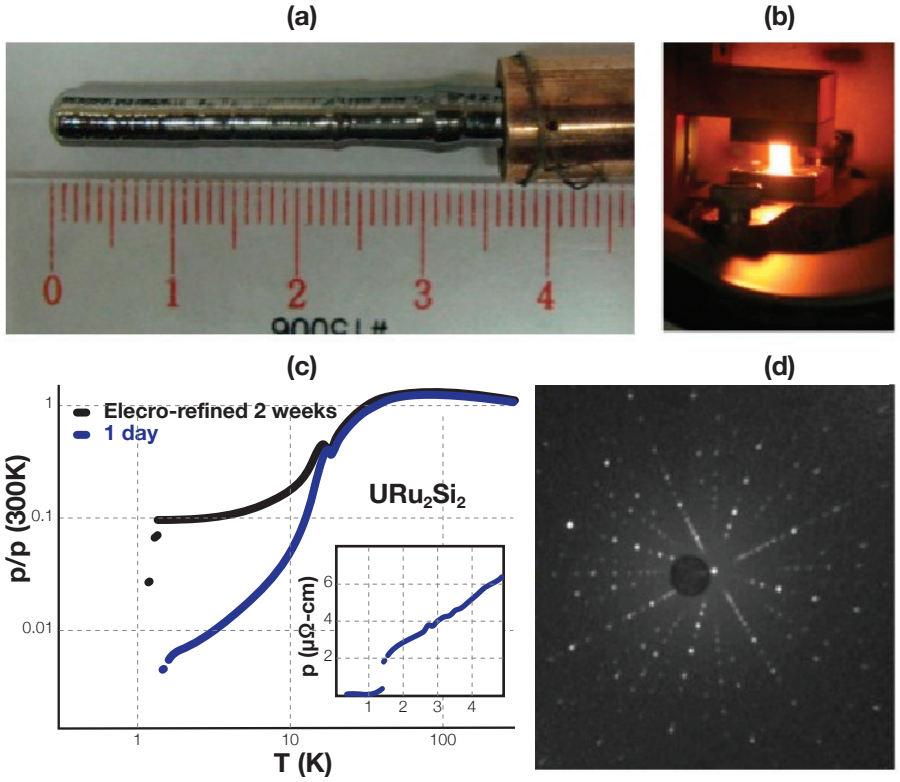

Figure 1: (a) A large single crystal of URu_2Si_2 grown by the Czochralski technique, (b) a piece of URu_2Si_2 at high temperature in the new electro-refiner setup, (c) the difference in crystal quality of URu_2Si_2 before and after electro-refinement. The inset shows the drop in resistance at the superconducting transition, and (d) a Laue diffraction pattern corresponding to a c-axis for URu_2Si_2.

the antiferromagnetic ordering temperature of UIr_4Al_{15} is shifted slightly to a higher temperature that suggests very little pressure dependence and a localized nature of the 5*f* electrons. The systems mentioned are only examples of the way in which these electronic ground states can manifest themselves.

The compounds URu_2Si_2 and $CePt_2In_7$ demonstrate how we are understanding correlated electron behavior of lanthanide and actinide systems. URu_2Si_2 is one of the familiar U ternary intermetallics that has gained attention over the past decade. It crystallizes with a tetragonal space group and shows superconductivity at 1.5 K as well as a "hidden order" transition at 17.5 K, which the origin of is still elusive. Both temperature features can be observed in a number of physical property measurements including magnetic susceptibility, heat capacity, and electrical resistivity. In addition to the questions surrounding the nature of this hidden order transition, another research group has shown that new states of matter can arise in very clean crystals of URu_2Si_2 with high purity.[5] We therefore embarked on a way to synthesize these very clean crystals in large enough quantities that would be suitable for measurements, such as nuclear magnetic resonance (NMR) and neutron diffraction, both of which would offer new insight into the intrinsic properties displayed by URu_2Si_2. At LANL, the MPA-CMMS group has developed a diverse synthesis infrastructure that includes not only the traditional arc-melting and metal flux growth techniques to grow large single crystals but also the ability to perform routine Czochralski growths using a tri-arc or induction coil furnace for high-temperature melts. Both of these capabilities allow for the preparation

of large neutron-sized single crystals for rare-earth-based and U-based compounds. We have also developed a unique capability for the purification of these large single crystals through electro-refinement. The technique involves passing a large current through the crystal that ultimately allows the crystal to reach about 90% of its melting point and drives the impurity phases from one end of the crystal to the other. We have assembled a system that can be used for all of the samples we produce in the tri-arc and induction furnaces, including Ce and U-based intermetallic compounds. Figure 1a shows the large single crystal of URu_2Si_2 grown in the tri-arc by pulling at a rate of 10 mm/hour. This crystal is then cut and a part is placed into the electro-refiner where it is shown at high temperature (Fig. 1b). Figure 1c is the data plot for our success in purifying a sample of URu_2Si_2 using the electro-refiner. There is a dramatic increase in RRR (a measure of crystal quality) upon electro-refining for 2 weeks. The resulting increase in overall crystal quality after refinement is shown in the plot of the as-cast and electro-refined material. Lastly, using the Laue diffraction method, Fig. 1d shows the typical diffraction pattern resulting from the crystallographic c-axis with the 4-fold symmetry expected from the tetragonal lattice of URu_2Si_2. The synthesized single crystals $CePt_2In_7$ is another compound that has opened the door for much more study both for the experimentalist and the theorist.[6] In recent years, numerous condensed matter physics groups have had an interest in the popular '115' family of compounds (these materials have a formula of RMX_5 where R = Ce or Pu, M = transition metal, and X = Ga or In). Their interest is justified because the Ce- and Pu-based materials offer instances of heavy fermion superconductivity and pressure-induced superconductivity.[7] From the physical property trends that are observed along this series comes an interesting crystal chemical interrelationship that connects the compounds. As can be seen from Fig. 2, the basic building block in the four named structure types is a $CeIn_3$ or $PuIn_3$ block. This building block is preserved in all of the compounds including the new $CePt_2In_7$. In fact a general formula may be written as follows where $Ce_mM_nIn_{3m+2n}$ [m = $CeIn_3$ layers,

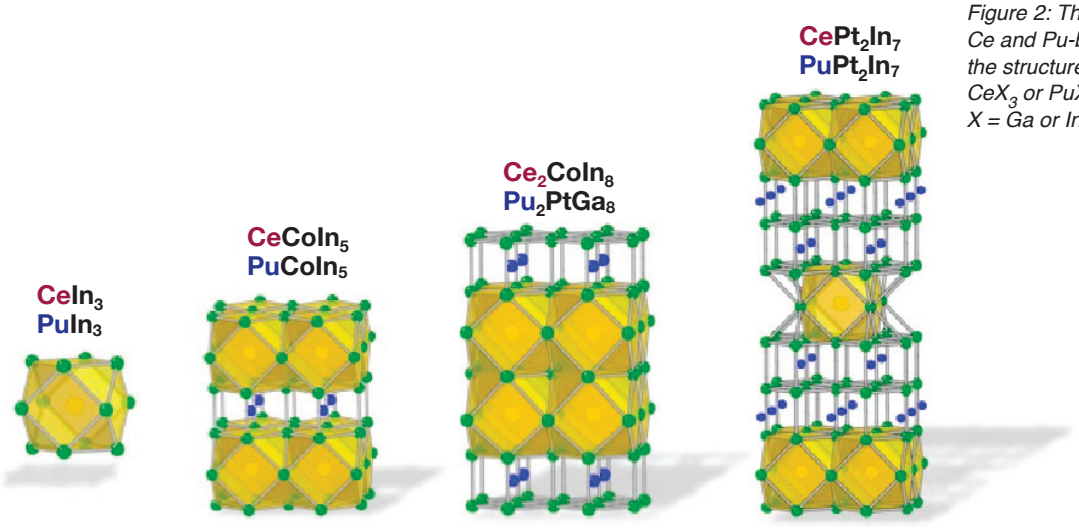

Figure 2: The four related structures of some Ce and Pu-based compounds. The similarity in the structures is realized by the building of the CeX_3 or PuX_3 moeities shown in yellow (where X = Ga or In).

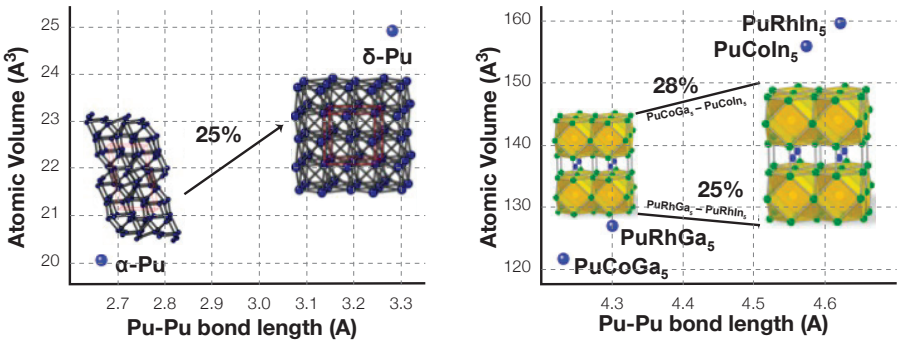

Figure 3: (left) Plot showing the difference in atomic volume for α-Pu and δ-Pu. (right) A similar situation is observed for the atomic volume difference between the Pu-based '115' materials. This comparison may offer insight into the emergence of intrinsic physical properties such as long-range magnetic order and superconductivity.

n = MIn_2 layers (M is a transition metal Co, Rh, Ir, Pd, or Pt)] and can be used to generate any of the four Pu ternary structures shown in Fig. 3. Having closely related families of compounds enables studying the interactions and intricate changes in the structure across the series of materials. Furthermore, the ability to substitute different elements onto unique crystallographic sites while remaining isostructural (maintain the same crystal structure) allows for accessing various electronic ground states for the rare earth or actinide atoms. In parallel efforts, we have also been able to extend this type of rationale for understanding correlated electron behavior in the realm of isostructural Pu compounds. We had success in synthesizing and characterizing these same four structure types using Pu and this offers a direct comparison to study both the 4*f* and 5*f* electrons, respectively. Recently, we have found long range magnetic order in $PuIn_3$ which undergoes antiferromagnetism at 14.5 K, superconductivity in $PuCoIn_5$ and $PuRhIn_5$ at 2.3 and 1.7 K.[8,9] The recent discovery of $PuCoIn_5$ offers the possibility for a direct comparison with the well-known $PuCoGa_5$ discovered in 2002. It should be noted that this compound still currently holds the record for the highest superconducting temperature (18.5 K) by a Pu intermetallic.[11] As shown in the right plot of Fig. 3, from $PuCoGa_5$ to $PuCoIn_5$ there is a nearly 28% increase in the unit cell volume. This is also true for the similar volume difference between $PuRhGa_5$ and $PuRhIn_5$. Both of these volume differences are similar to what occurs between α-Pu and δ-Pu (a volume difference of ~25%) so it serves as a logical way to probe the 5*f* electrons and Pu-Pu interatomic interactions in elemental Pu and Pu intermetallic compounds. The volume expansion between the intermetallic compounds is expected to localize the Pu 5*f* electrons in $PuCoIn_5$ as compared with the isostructural and more delocalized $PuCoGa_5$. It is often suggested that the larger unit cell volume of δ-Pu arises from the emergence of magnetic moments present there. However, the recent work by Lashley and collaborators shows no evidence for localized magnetic moments as suggested by magnetic susceptibility studies.[11]

Currently it is known that the 5*f* electrons of elemental Pu cannot be treated as purely itinerant or localized but in fact sit between both extremes. This has been notoriously called "the correlated electron problem" of plutonium. Now, more than ever, it is widely recognized that the 94th element in the periodic table, plutonium, is possibly the most complex of all elements. This suggestion arises from the variation of its physical and electronic properties, e.g., its brittle and ductile nature depending on its crystal structure and absence of local magnetism. In its simplest elemental

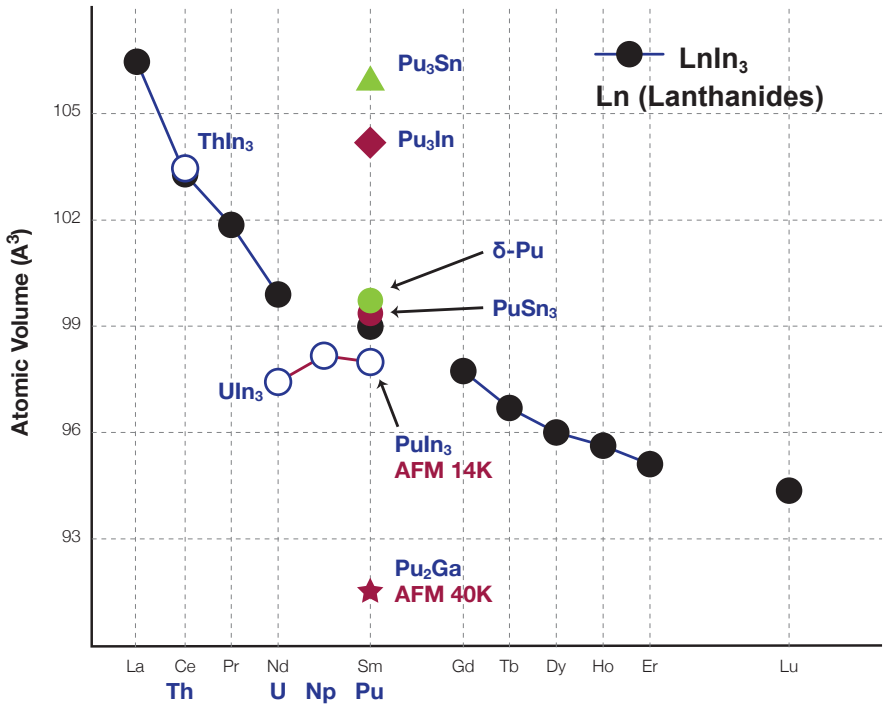

Figure 4: Plot of the trends in atomic volume for some Pu binary compounds in hopes to shed insight into the observed physical properties. As a comparison, the steady decrease of atomic volume for the related $LnIn_3$ compounds displays the usual lanthanide contraction as one moves left to right across the series.

form, it can exist in six allotropic configurations ranging from low symmetry monoclinic structures to high symmetry cubic structures. This only serves to show how plutonium's structural chemistry can adapt to various coordination environments. When it composes an intermetallic compound, we not only see a span of structural chemistries (high symmetry cubic and tetragonal phases to low symmetry monoclinic phases), but also a myriad of electronic ground states. Perhaps the biggest question that needs to be answered is how to understand the true nature of the 5*f* electrons in Pu, which has been shown to exhibit both itinerant (delocalized) or localized behavior depending on its electronic configuration.

Having single crystals of various Pu allotropes would allow researchers to address this issue, but it has proved not so easy because of the complicated phase space and stability of the structures. To circumvent this, we can instead produce crystals of Pu intermetallics, which can be directly compared with the allotropes of elemental Pu through a crystallographic analysis (similar coordination environments, bond distances, and building block units) as well as physical properties. As shown in Fig. 4, plotting the atomic volumes for some of the known Pu binary compounds (two of which show magnetic order) offers suggestions as changing Pu-Pu bonding interactions that can be possibly correlated to δ-Pu. Figure 5 shows the structures of two binary Pu compounds with In. These compounds have the formulae $PuIn_3$ and Pu_3In and both crystallize in the identical space group Fm-3m in the $AuCu_3$ structure type. Our interest in these, as well as in isostructural compounds with various p-block metals, stems from their close relationship to δ-Pu. We plan to study phase relationships of these systems in hopes of gaining awareness of the intricate structure and bonding in these

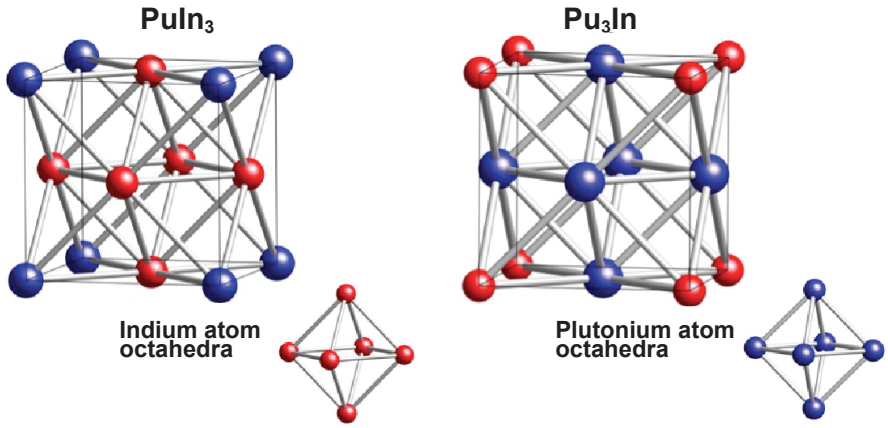

Figure 5: The unit cell structures of $PuIn_3$ and Pu_3In, which are composed of In or Pu octahedral, respectively. These materials are of interest not only for better understanding phase stability of the Pu-X binary phase diagrams but also for the close relation to δ-Pu.

materials as well come closer to an answer explaining the missing magnetism in α-Pu and δ-Pu. To summarize, the three main questions this approach will address are as follows:

- What is the true electronic ground state of Pu?
- Can we harness the conditions for stability and thermodynamics of Pu alloys and compounds?
- How is the magnetism of the 5*f* electrons related to crystal structure and valence states?

Of course, this direction will only prove to be useful by further increasing the number of examples of novel intermetallic compounds. The crystal chemistry of Pu offers a range of structure and bonding arrangements for Pu, which suggests a number of electronic ground states for Pu. For more information, see a recent review[9] of LANL's synthetic infrastructure and capability for the preparation, characterization, and measurement of Pu single-crystal intermetallics and alloys.

Further Reading:

1. *Integrated Plutonium Science and Research Strategy, LAUR-13-24336, Los Alamos National Laboratory, Lawrence Livermore National Laboratory.*
2. *P. H. Tobash, F. Ronning, J.D.Thompson, S. Bobev, and E.D. Bauer, "Magnetic order and heavy fermion behavior in CePd1+xAl6–x: Synthesis, structure, and physical properties", J. Solid State Chem. 183, 2010.*
3. *P. H. Tobash, Y. Jiang, F. Ronning, C.H. Booth, J.D. Thompson, B.L. Scott, and E.D. Bauer, "Synthesis, structure, and physical properties of YbNi3Al9.23", J. Phys. Cond. Mat. 23, 2011.*
4. *P. H. Tobash, B.L. Scott, V.E. Sidorov, F. Ronning, K. Gofryk, J.D. Thompson, R.C. Albers, J.H. Zhu, J.W. Jones, and E.D. Bauer, "Heavy Fermion Behavior in the New Antiferromagnetic Compound UIr4Al15", J. Phys. Conf. Series 273, 2011.*
5. *T.D. Matsuda, D. Aoki, S. Ikeda, E. Yamamoto, Y. Haga, H. Ohkuni, R. Settai, and R. Onuki, "Super Clean Sample of URu2Si2", J. Phys. Soc. Jpn. 77, 2008.*
6. *P. H. Tobash, F. Ronning, J.D. Thompson, B.L. Scott, J.H. Moll, B. Batlogg, and E.D. Bauer, "Single crystal study of the heavy-fermion antiferromagnet CePt2In7", J. Phys. Cond. Mat. 24, 2012.*
7. *J.L. Sarrao and J.D. Thompson in J. Phys. Soc. Japan 76, 2007.*
8. *E.D. Bauer, M.M. Altarawneh, P. H. Tobash et al., "Localized 5f electrons in superconductng PuCoIn5: consequences for superconductivity in PuCoGa5", J. Phys. Cond. Mater. 24, 2012.*
9. *E.D. Bauer, P. H. Tobash, J.N. Mitchell, and J.L. Sarrao, "Single crystal growth of plutonium compounds from modten metal fl uxes", Phil. Mag. 92, 2466–2491, 2012.*
10. *J.L. Sarrao, L.A. Morales, J.D. Thompson, B.L. Scott, G.R. Stewart, F. Wastin, R. Rebizant, P. Boulet, E. Colineau, and G.H. Lander, "Plutonium-based superconductivity with a transition temperature above 18 K", Nature 420, 297–299, 2002.*
11. *J.C. Lashley, A. Lawson, R.J. McQueeney, and G.H. Lander "Absence of magnetic moments in plutonium", Phys. Rev. B 72, 2005.*

Screened Hybrid Functional Predictions on Actinide Oxides, Nitrides, and Carbides

Actinide materials, such as actinide oxides, nitrides, and carbides, are challenging systems for both experiment and theory. Due to their toxicity and radioactivity, they are difficult to characterize experimentally. From a theoretical perspective, these materials are strongly correlated systems that have incompletely filled *f* orbitals, and can not be well described by simple one-electron theories such as density functional theory (DFT) or Hartree-Fock (HF) theory. Each single electron in the strongly correlated materials has a direct influence on its neighbors instead of contributing only to the averaged motion of the others. In general, the actinide oxides fall into strongly correlated insulators that can not conduct an electric current. Actinide oxides (UO_2, PuO_2, their mixed oxide, etc.) have been used as nuclear fuels in industry for many years. The nitrides and carbides are generally strongly correlated metals (conducting electricity). This generally means they also conduct heat well, making them ideal fuel candidates for certain Generation IV reactors.

DFT is a quantum mechanical modeling method used in physics and chemistry to investigate the electronic structure of a material. The 1998 Nobel Prize in chemistry was awarded to Walter Kohn for his development of DFT and to John A. Pople for his development of computational methods in quantum chemistry. DFT has been extensively used to predict material properties. DFT is supported by many quantum chemistry and solid state physics suites of software such as the Vienna Ab initio Simulation Package (VASP), QUANTUM-ESPRESSO, ABINIT, GPAW, Gaussian, WIEN2k, and ELK.

DFT is in principle an exact theory. However, the major problem with DFT is that the exact functional for exchange and correlation is not known, which leads to a hierarchy of approximations, including the local-density approximation (LDA), generalized gradient approximations (GGA), and hybrid functionals. The first three generations of functionals (LDA, GGA, and meta-GGA) are incapable of accurately describing actinide oxides' electronic structures. For instance, they predict UO_2 (a Mott insulator with 2.1 eV band gap in experiment) to be a metal. In fact, the development of more accurate functionals has become the bottleneck for the future applications of DFT. The problem is due to an overestimation of the self-interaction energy in these DFT functionals, the so-called "self-interaction errors". In the HF method, the self-interaction energy is exactly cancelled.

A fourth generation of DFT, the hybrid functionals (such as PBE0), which incorporate a portion of exact exchange from HF theory, partially reduce the self-interaction errors and met with successes for Mott insulators. For instance, the simplest hybrid functional, PBE0, predicts UO_2 to be an

Xiao-Dong Wen

This paper was contributed by Xiao-Dong Wen, Richard L. Martin, Gustavo E. Scuseria, Sven P. Rudin, and Enrique R. Batista, Xiao-Dong Wen was a Seaborg postdoc from June 2011–May 2013. His area of study was first principles prediction for strongly correlated materials: a screened hybrid DFT study, with mentor Richard Martin of T-1. Xiao-Dong is now a staff member in T-1, Physics and Chemistry of Materials.

anti-ferromagnetic insulator. However, the functional shows some problems on metallic systems such as UN.

The Heyd-Scuseria-Ernzerhof (HSE) functional—also called screened hybrid functional—uses a screened Coulomb potential to calculate the exchange portion of the energy in order to improve computationally efficiency, especially for metallic systems. In screened hybrids, the concept of range separation takes center stage, as the interelectronic Coulomb potential is split into short range (SR) and long range (LR) components:

$$\frac{1}{r_{12}} = S_\omega(r_{12}) + L_\omega(r_{12}) = \frac{erfc(\omega r_{12})}{r_{12}} + \frac{erf(\omega r_{12})}{r_{12}}$$

where the interelectronic distance is $r_{12} = |\vec{r}_1 - \vec{r}_2|$, erf is the error function and governs long-range behavior, *erfc* is its short–range complement, and the screening length ω determines the extent of short-range interactions. The functional can be expressed as:

$$E_{xc}^{HSE} = aE_x^{HF,SR}(\omega) + (1-a)E_x^{PBE,SR}(\omega) + E_x^{PBE,LR}(\omega) + E_c^{PBE}$$

a = ¼ where $E_x^{HF,SR}$ is the full non-local HF short-range exchange interaction, $E_x^{PBE,SR}$ and $E_x^{PBE,LR}$ are a semi-local short-range and long-range exchange interaction from the conventional PBE approximation to DFT, respectively, and E_c^{PBE} is the corresponding PBE correlation energy. This functional has proven very useful for studies of semiconductors and insulators, particularly for the calculation of reliable band gaps and lattice constants.[1]

HSE does not require the introduction of any material-specific parameters (a=25% and ω=0.207 for all materials), and has had considerable success in describing important features of the actinide oxides when compared with available experimental data. However, it still needs further improvement to describe strongly correlated metals, such as UN and UC. In this article, we review our recent work on the predictions of HSE for actinide materials, including oxides, nitrides, and carbides.

Part I: Actinide Oxides

We have systemically explored the performance of the screened hybrid functional HSE in the actinide oxides series. We conclude that HSE gives a reasonable reproduction of the electronic and optical properties for these actinide dioxides when compared with available experimental data, recently obtained by our experimental collaborators at LANL: Thomas M. McCleskey, Brian L. Scott, Eve Bauer, John J. Joyce, Tomasz Durakiewicz, Steven D. Conradson, Quanxi Jia, and Stosh A. Kozimor.[2]

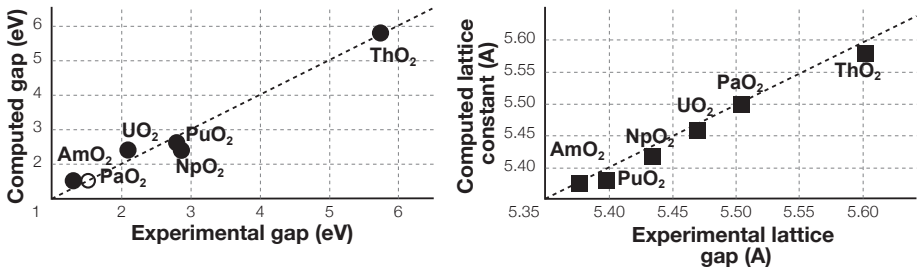

Figure 1: Theory vs Experiment. Optical band gaps (left panel) and lattice constants (right panel) for the series of actinide dioxides AnO_2 (An=Th, Pa, U, Np, Pu, and Am).

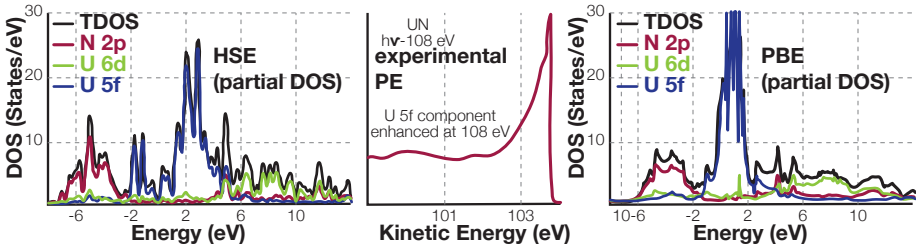

Figure 2: Calculated density of states (DOS) of AFM rocksalt UN by HSE (left panel) and PBE (right panel), as well as the experimental PES (middle panel) enhanced at 108 eV.

As mentioned earlier, HSE does not require the introduction of any material-specific parameters. The computed HSE lattice constants and band gaps of AnO_2 are in consistently good agreement with the available experimental data across the series (Fig. 1). ThO_2 is a simple band insulator (f^0), while PaO_2, UO_2, and NpO_2 are predicted to be Mott insulators (the lowest excitation is from an occupied to an unoccupied f orbital); O 2p states are well separated from the f states, indicating more ionic bonding (see Fig. 2 left). The remainder of the series (PuO_2, AmO_2 and CmO_2) show considerable O 2*p*/An5*f* mixing (see Fig. 2 right) and are classified as charge-transfer insulators (the lowest excitation is from the O 2p ligand band to an unoccupied f-orbital). These materials exhibit more covalent bonding.[3]

The screened hybrid functional has met remarkable success not only on AnO_2 series, but also on α-U_3O_8.[4] The calculations predicts one U(VI) and two U(V) sites in α-U_3O_8, and a band gap of 0.8 eV, which is close to the experimental value obtained by our team.

Part II: Actinide Nitrides

While the screened hybrid HSE functional seems clearly superior for the strongly correlated actinide dioxide insulators, its performance for the metallic nitrides is problematic, at least with respect to the densities-of-states.[5] Let's take UN as an example. HSE correctly predicts it to be metallic. The density of states of UN obtained with a simple GGA, PBE, compares well with the experimental photoemission spectra (see Fig. 2), in contrast to the screened hybrid approximation, which significantly underestimates the DOS near the Fermi energy. This is presumably related to the need of additional screening in the Hartree-Fock exchange term of the metallic phases. In a metal, one expects the Coulomb interactions to be more effectively screened than in an insulator. The screening length, ω, governs the range of the Hartree-Fock exchange term; the optimum value obtained from many tests on small molecules is approximately 0.2-0.3 $Å^{-1}$, or a range of roughly 5 Å. For HSE it is fixed at its standard value of 0.207 $Å^{-1}$. It is well known, however, that the range should in principle be much shorter in a metal. To test the sensitivity of our results to the range parameter ω, we find that the density at the Fermi level increases with an increase of the screening parameter, or a shorter range for the exchange term. The solution to our problem is not to adjust the screening length for each new metal we address, for that destroys the desired predictive nature of screened DFT. One avenue that might correct this problem is to develop an approach in which the screening parameter is determined and adjusted dynamically as the calculation proceeds.

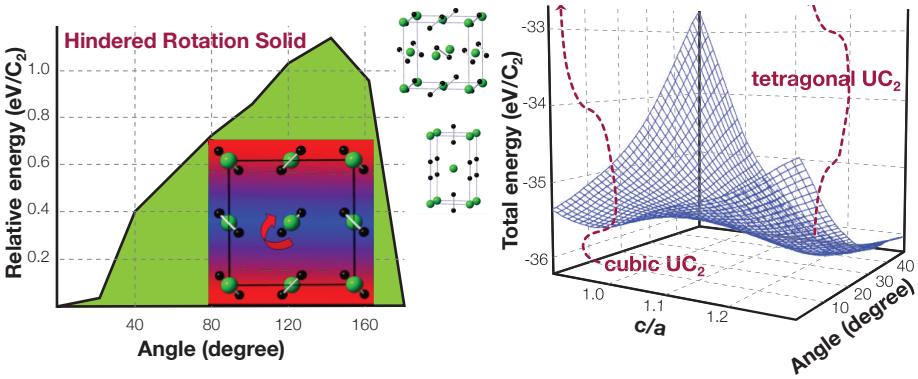

Figure 3: The rotational energy barrier (left) and phase transition (right) of hindered rotational solid UC_2.

Part III: Actinide Carbides

We have explored the screened hybrid approximation on uranium dicarbide (UC_2 with C_2 units). The cubic UC_2, a high temperature phase calculated to be a paramagnetic semiconductor with a narrow gap, 0.4 eV. This phase contains C_2 units with a computed C-C distance of 1.443 Å, which is in the range of a CC double bond; U is formally in 4+, C_2 in 4-. Interestingly, the C_2 units connecting two uranium sites can rotate freely (with low energy barrier, less than 0.05 eV per UC_2) up to an angle of 30°, indicating a hindered rotational solid (see Fig. 3 left). Here, we would like to say more about rotational solids, such as solid H_2 and solid CH_4, which have been known for some time. In these materials, the individual molecular units in the solid can be rotated about their center of mass essentially freely or at least partially so; such rotational behavior is usually associated with molecular crystals. In this work, we found this behavior in an inorganic solid crystal, and suggested that the rotational behavior might affect its thermal conductivity.

Ab-initio molecular dynamics simulations based on HSE show that the rotation of C_2 units in the low-temperature phase (tetragonal UC_2) occurs above 2000 K, in good agreement with experiment (characterized by LANL LANSCE researcher Sven C. Vogel). The computed energy barrier for the phase transition from tetragonal UC_2 (low-temperature phase) to cubic UC_2 (high-temperature phase) is around 1.30 eV per UC_2 (see Fig. 3 right).[6]

The development of HSE has provided new and exciting insights into the fundamental chemistry and physics of these strongly correlated insulators. However, there is still work to be done with the primary need for further improvement being associated with the ability to describe strongly correlated metals.

Acknowledgement

This work was supported under the Heavy Element Chemistry Program at Los Alamos National Laboratory by the Division of Chemical Sciences, Geosciences, and Biosciences, Office of Basic Energy Sciences, U.S. Department of Energy. Portions of the work were also supported by the LDRD program at Los Alamos National Laboratory. Xiao-Dong Wen gratefully acknowledges a Glenn T. Seaborg Institute Fellowship. The work at Rice University is supported by DOE, Office of Basic Energy Sciences,Heavy Element Chemistry program, under Grant DEFG02-04ER15523. Gustavo E. Scuseria is a Welch Foundation Chair (C-0036). Some of the calculations were performed on the Chinook computing systems at the Molecular Science Computing Facility in the William R. Wiley Environmental Molecular Sciences Laboratory (EMSL) at PNNL. Some of the calculations were done on the Lobo supercomputer, operated by the High Performance Computing Division at Los Alamos National Laboratory.

References:

1. *J. Heyd, G.E. Scuseria, M. Ernzerhof, "Hybrid functionals based on a screened Coulomb potential", J. Chem. Phys. 2003, 118, 8207 and J. Chem. Phys. 2006, 124, 219906.*
2. *J.L. Musfeldt, T.V. Brinzari, J.A. Schlueter, J.L. Manson, A.P. Litvinchuk, Z. Liu, "Pressure-induced local lattice distortions in α-Co[N(CN)2]2", J. Appl. Phys. 2013, 113, 13515.*
3. *X.-D. Wen, R. L. Martin, G.E. Scuseria, S.P. Rudin, E.R. Batista, "A Screened Hybrid DFT Study of Actinide Oxides, Nitrides, and Carbides", Chem. Rev. 2013, 113, 1063-1096 and J. Chem. Phys. 2012, 137, 154707.*
4. *X.-D. Wen, R.L Martin, G.E. Scuseria, S.P. Rudin, E.R. Batista, A.K. Burrell, "Screened hybrid and DFT + U studies of the structural, electronic, and optical properties of U3O8", J. Phys. Condens. Matter 2012 25(2), 025501.*
5. *X.-D. Wen, R.L. Martin, G.E. Scuseria, S.P. Rudin, E.R. Batista, "A Screened Hybrid DFT Study of Actinide Oxides, Nitrides, and Carbides", J. Phys. Chem. C, 2013 117, 13122–13128.*
6. *X.-D. Wen, S.P. Rudin, E.R. Batista, D.L. Clark, G.E. Scuseria, R.L. Martin, "Rotational Rehybridization and the High Temperature Phase of UC2, Inorganic Chemistry, 2012 51, 12650-12659.*

Seaborg Institute hosts West Point Cadet Steven Sloan

This article was contributed by Patrice Stevens of the LANL Seaborg Institute, mentor to Cadet Steven Sloan during his SARA internship at LANL in 2013.

Steven Sloan was one of seventeen cadets from United States military academies to come to Los Alamos National Laboratory as part of the 2013 Service Academy Research Associate (SARA) program. A goal of the SARA program is to introduce students at three service academies (West Point, Annapolis, and the U.S. Air Force) to Los Alamos National Laboratory as a resource for future endeavors that cadets will face as military officers. West Point Cadet Sloan had the opportunity to work with scientists and engineers at the Laboratory's Plutonium Facility (PF-4) for four weeks this summer. Steven's area of focus was radioactive material and in particular plutonium-238. He already held an active security clearance, which made his choice possible. Patrice Stevens of the Glenn T. Seaborg Institute was his technical mentor. His experience inside PF-4 was very relevant to his West Point courses in nuclear engineering, including heat transfer, instrumentation and shielding, and dynamics of nuclear effects.

Steven worked with LANL engineers in capturing the overall process of plutonium oxide pellet formation to determine if any process steps could be eliminated or modified to increase production efficiency while still maintaining the rigorous quality standards. Preparation of plutonium-238 oxide pellets requires several processing operations with numerous steps. The first operation is to purify the plutonium and remove the impurities. The purification process occurs during an aqueous operation and requires

Steven Sloan demonstrates the proper procedure of monitoring anti-contamination clothing prior to exiting a laboratory in PF-4. Louis Jaramillo assists with the monitoring process.

Cadet Sloan observes machining of plutonium at PF-4.

***An RTG converts heat** generated by the radioactive decay of plutonium-238 into electricity, taking advantage of the Seebeck effect. The Seebeck effect harnesses a natural phenomenon: metals respond to heat differently, and that enables a thermoelectric circuit in a loop of unlike conductors. RTGs using plutonium-238 as a heat source are invaluable deep space exploration components because they are a reliable source of electricity when solar electric generation is not possible.*

the final product to have tight tolerances ensuring that even small amounts of impurities are removed. During the fuel processing and pellet fabrication operations, a homogenous particle size is required. The particle size is very small. If a glovebox is breached, the principal hazard is a worker uptake of the small plutonium particles. Therefore, it is important to carefully follow the glovebox procedures. One of Steven's assignments was to investigate ways to reduce potential worker exposure to hazardous material by allowing for a larger particle size during pellet fabrication. Steven spent time in the PF-4 learning about the physical and chemical differences of plutonium isotopes and their uses, specifically, the heat source manufacturing process operations, including the purification of plutonium-238 oxide, fuel processing and pellet fabrication, heat source encapsulation, and nondestructive testing required for quality assurance. He became familiar with the conduct of operations for operating and performing work in a Security Facility Category I, High Hazard Category II Nuclear Facility such LANL's Plutonium Facility. He was especially interested in plutonium-238 as a heat source material used in radioisotope thermoelectric generators (RTGs), in particular the application of this material to civil engineering problems. Steven is keeping his options open as he looks forward to graduation in May 2014 and the required 5 years of active duty. "I don't want to paint myself into a corner," he said. His long-term goal is "to solve problems", and it is clear that that is exactly what he is going to do.

2013 LANL Seaborg Post-docs

Name	Project	Mentor
Beau Barker	*Spectroscopic investigations of actinyl species*	*Marianne Wilkerson, C-NR*
Olga Batuk	*Science of defects in materials*	*Steve Conradson, MST-8*
Leah Broussard	*Actinide Studies using ultra-cold neutrons*	*Mark Makela, P-25*
Xiaoyan Chen	*Actinide Chemistry in functionalized ionic liquids*	*George Goff, Wolfgang Runde, C-IIAC*
Magen Coleman	*Development of a two-dimensional system for mapping gamma-emitting radionuclides in support of forensic examination*	*Lav Tandon, C-AAC*
Jason Ellis	*Materials for studying 229^{th} nuclear transitions using optical spectroscopy*	*Rich Martin, T-1*
Heming He	*Molecular forensics science of nuclear materials*	*George Goff, Wolfgang Runde, C-PCS*
Marko Knezevic	*Modeling deformation of α-uranium with embedded polycrystal formulations in finite elements*	*Bogdon Mihaila, MST-6*
Georgios Koutroulakis	*239Pu nuclear magnetic resonance on Pu-based compounds*	*Joe Thompson, MPA-CMMS*
Alejandro Lichtscheidl	*Synthetic approaches to the isolation and characterization of uranium alkylidene complexes*	*Jackie Kiplinger, MPA-MSID*
Kathryn McIntosh	*Development of complementary XRF analytical methods for characterization of actinide elements*	*George Havrilla, C-CDE*
Stefan Minasian	*Development of light-atom ligand K-edge X-ray absorption spectroscopy*	*Stosh Kozimor, C-IIAC*
Angela Olson	*Investigation of covalency in dithiophosphinate actinide extractants using S K-edge X-ray absorption spectroscopy*	*Stosh Kozimor, C-IIAC*
Arkady Shehkter	*Phonon-driven electron localization in a-plutonium*	*Albert Migliori, NSEC*
Floyd Stanley	*Next-generation plutonium materials analysis via the refined development and application of a novel TIMS ionization source*	*Khalil Spencer, C-AAC*
Neil Tomson	*Synthesis and study of imido analogs to UO3*	*Jim Boncella, MPA-MSID*
Nicholas Travia	*Activation of thiophene derivatives by actinide complexes and relevance to hydrodesulfurization*	*Jackie Kiplinger, MPA-MC*
Xiaodong Wen	*First principles prediction for strongly correlated materials: a screened hybrid DFT study*	*Rich Martin, T-1*
Justin Wilson	*Investigating the chemistry of actinium-225, a therapeutic radionuclide*	*Eva Birnbaum, C-IIAC*
Ryan Winkler	*High-precision study of gamma-ray emission following the α-decay of 242Pu*	*Michael Rabin, ISR-2*

Las Vegas, Nevada
Ranaissance Hotel
September 7-12, 2014

THE SCIENCE 2014

Topical Areas

- Condensed matter physics
- Compounds and complexes
- Surface science and corrosion
- Aging and phase stability
- Materials science
- Detection and analysis
- Nuclear fuel cycle
- Environmental chemistry
- Coordination chemistry
- Solution chemistry

Conference Special Events

- Tutorial session
- Banquet speaker: Former U.S. Secretary of Defense, Dr. William Perry
- Nevada National Security Site tour

Abstracts due: March 14, 2014

Authors are invited to submit abstracts at:
www.ans.org/meetings/pu

For additional information, contact the conference organizers:

Kerri Blobaum: blobaum1@llnl.gov
Scott McCall: mccall10@llnl.gov